

Article

Zircon Hf-Isotopic Mapping Applied to the Metal Exploration of the Sanjiang Tethyan Orogenic Belt, Southwestern China

Bin Du ^{1,2}, Zian Yang ^{1,*}, Lifei Yang ³, Qi Chen ², Jiaxuan Zhu ², Kangxing Shi ², Gao Li ¹, Lei Wang ¹ and Jia Lu ¹

¹ China Non-Ferrous Metals Resource Geological Survey, No.5 Courtyard Area 4, Anwai Beiyuan, Chaoyang District, Beijing 100012, China; dubin6866@126.com (B.D.); bj_ligao@126.com (G.L.); wla2009@sina.cn (L.W.); chnlujia@163.com (J.L.)

² State Key Laboratory of Geological Processes and Mineral Resources, China University of Geosciences, No. 29 Xueyuan Road, Haidian District, Beijing 100083, China; dirk@cugb.edu.cn (Q.C.); 3001190005@cugb.edu.cn (J.Z.); shikx@email.cugb.edu.cn (K.S.)

³ School of Earth of Sciences, East China University of Technology, 418 Guanglan Road, Nanchang 330013, China; lfyang@ecut.edu.cn

* Correspondence: yzaldy88@126.com; Tel./Fax: +86-10-84925807

Abstract: Zircon Hf-isotopic mapping can be regarded as a useful tool for evaluating the coupling relationship between lithospheric structure and metallic mineralization. Hence, this method shows important significance for mineral prediction. To explore this potential, the published granite zircon Hf isotope data from the Sanjiang Tethyan Orogen were systematically compiled. This study uses the Kriging weighted interpolation in the Mapgis software system to contour Hf isotopes, revealing a relation between the crustal structure and metallogenesis. The mapping results suggest that the Changning–Menglian suture zone is the boundary between ancient and juvenile crust, viz., the western terranes have ancient crust attributes, whereas the eastern terranes exhibit the properties of new juvenile crust. In addition, this study also found that the mineralization and element types in the Sanjiang Tethyan Orogen have a coupling relationship with the crustal structure. The distribution of porphyry Cu–Mo–Au deposits is mainly controlled by the new juvenile crust, whereas the magmatic-hydrothermal Sn–W and porphyry Mo–W(-Cu) deposits are closely related to the reworked ancient crust. The results of zircon Hf isotope mapping prove that the formation and spatial distribution of deposits are related to the composition and properties of the crust. Hf isotope mapping can reveal the regional metallogenic rules and explore metallogenic prediction and metallogenic potential evaluation.

Keywords: Hf isotope mapping; mineral exploration; Sanjiang Tethyan orogenic belt



Citation: Du, B.; Yang, Z.; Yang, L.; Chen, Q.; Zhu, J.; Shi, K.; Li, G.; Wang, L.; Lu, J. Zircon Hf-Isotopic Mapping Applied to the Metal Exploration of the Sanjiang Tethyan Orogenic Belt, Southwestern China. *Appl. Sci.* **2022**, *12*, 4081. <https://doi.org/10.3390/app12084081>

Academic Editor: Andrea L. Rizzo

Received: 26 February 2022

Accepted: 14 April 2022

Published: 18 April 2022

Publisher's Note: MDPI stays neutral with regard to jurisdictional claims in published maps and institutional affiliations.



Copyright: © 2022 by the authors. Licensee MDPI, Basel, Switzerland. This article is an open access article distributed under the terms and conditions of the Creative Commons Attribution (CC BY) license (<https://creativecommons.org/licenses/by/4.0/>).

1. Introduction

Standard methods of geological prospecting include regional geological mapping, geophysical [1,2] and geochemical surveys [3,4], remote sensing [5–9], and aerial surveys [10–12]. These traditional geological methods have found many deposits, but they also have serious shortcomings, which are costly and challenging for finding mineral deposits. Therefore, new methods need to be developed to explore potential mineral deposits [13–15].

In recent years, regional isotope tracer mapping methods have been widely used to evaluate accretionary and collisional orogeny processes [16–18], describe regional lithospheric three-dimensional architectures [16,19], constrain geotectonic boundaries [17,18,20–24], define the compositions and properties of deep geotectonic units [25,26], surmise the crustal growth [26], and reveal the distribution of mineral deposits [16–18,20–24,27]. Hence, this method shows important significance in mineral exploration and prediction. The Sanjiang Tethyan orogenic belt is located on the southeastern margin of the Tibetan Plateau, belonging to the combined zone of Gondwana and ancient

Eurasia (Figure 1). It has experienced Proto-, Paleo-, Meso-, and Neo-Tethyan evolution and the subsequent oblique continental collision [17,28–32]. Correspondingly, this belt has formed episodic and diverse metallogeny with the tectonics evolved from Tethyan accretionary orogenesis to collisional orogenesis [32–34]. Therefore, the Sanjiang Tethys domain is a natural laboratory for exploration and prospecting for deposits. However, the evolution and structure of the continental lithosphere that controls the localization of ore deposits still remain poorly understood.

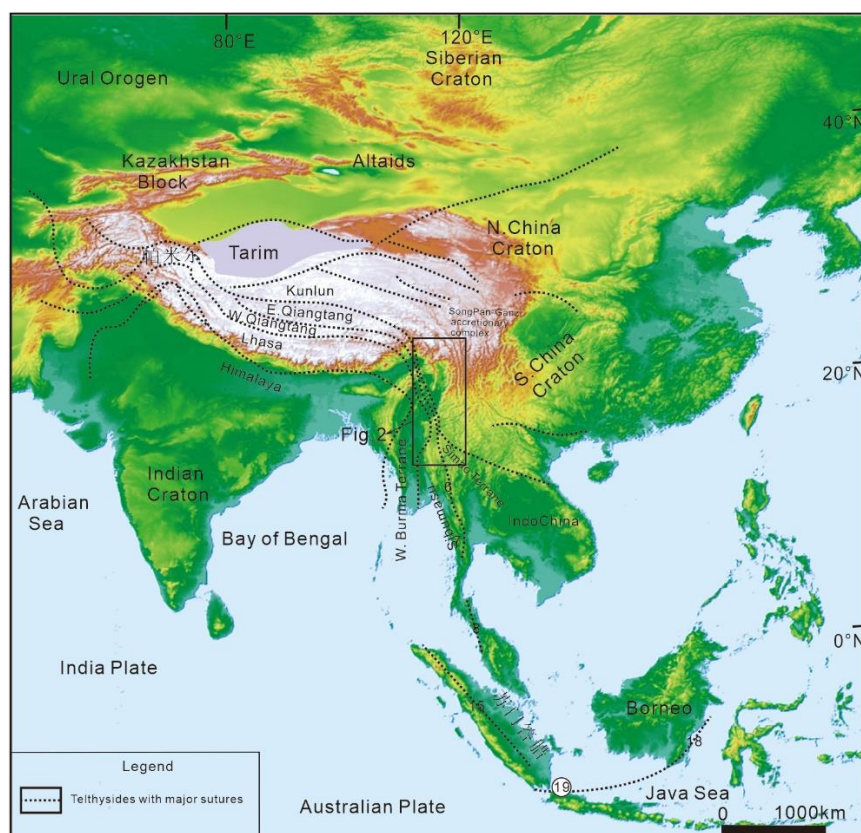


Figure 1. Geological map showing the tectonic framework of the Sanjiang Tethyan Orogen and its adjacent areas. Adapted with permission from Ref. [17]. Copyright 2016 ELSEVIER.

In this paper, based on the reviews of the previous zircon Hf-isotopic research, we use the zircon Hf isotope mapping method to explore the genetic relationship between the tectonic evolution and various deposits in Sanjiang Tethyan orogenic belt. This study also summarizes the distribution of different deposits in the area and provides a theoretical basis for the following mineralization and exploration.

2. Hf Isotope Mapping's Application to Mineral Prospection

In recent years, some researchers have made more attempts to use zircon Hf isotope mapping to explore the resolution of the three-dimensional tectonic framework and mineralization pattern, mainly focusing on the regions of the Yilgarn Craton of Western Australia, the Lhasa terrane in China, the Eastern Qinling Orogen, and the North China Craton [16,20,22–24,27,35].

Mole et al. [20] performed regional zircon Hf isotopic mapping of the Yilgarn Craton of Western Australia and found that the distribution of magmatic-related deposits is closely related to the formation of material from earth's deep mantle and the new crust. Hou et al. [16] conducted zircon Hf-isotopic mapping of regional magmatic rocks in the Lhasa terrane, revealing that the upper lithosphere material structure and composition of the Lhasa terrane are consistent with the deposit distribution of the Gangdese metallogenic

belt. The porphyry Cu(-Mo-Au) deposits are all distributed in the positive zircon $\epsilon\text{Hf(t)}$ area, which is associated with the juvenile crust formation in the South and North Lhasa sub-terrane. Granite-related Pb-Zn deposits are typically localized along the margin of the old crustal block bounded by lithospheric faults. The oldest crustal region developed along the margin of the old crustal block is bounded by lithospheric faults, which is in the negative zone of zircon $\epsilon\text{Hf(t)}$. The Hf isotope mappings show that the juvenile crust has a primary control on the formation of porphyry Cu(-Mo-Au) deposits. The distribution of Pb-Zn-Mo deposits in the central sub-terrane is constrained by the inhomogeneity of the composition of ancient crustal blocks and remelting or reworking. Wang et al. [22] revealed that the formation of porphyry and porphyry-skarn Mo(-W) deposits are closely related to the remelting of the ancient crust through zircon Hf isotope mapping of the east Qinling orogen. Wang et al. [23] studied the zircon Hf isotope mapping of the North China Craton and found that the formation of BIF-type iron deposits is associated with the remelting modification of ancient crust, and the formation of orogenic gold deposits is related to the formation of juvenile crust [36]. Deng et al. [24] demonstrated that isotope mapping can constrain the distribution pattern of large-scale gold deposits by conducting zircon Hf isotope mappings of magmatic rocks in the southeast North China Craton. Jiao Dong-type gold deposits and porphyry-skarn Mo(-W-Cu) deposits are typically localized at regions with negative $\epsilon\text{Hf(t)}$ values, showing an ancient crustal base composition. Porphyry-skarn Cu(-Au-Mo) deposits in the west of Shandong province cluster variable $\epsilon\text{Hf(t)}$ values, showing an ancient crustal and juvenile crustal composition, indicating the contribution of mantle-derived material to mineralization.

3. Geologic Setting

The Sanjiang (Three Rivers) region is named due to it being drained by three major rivers: the Jinshajiang, Lancangjiang, and Nujiang [17,30]. The region is the eastern segment of the Tethys-Himalayan tectonic domain, covering the southeastern part of the Tibetan Plateau and the western part of Yunnan Province (Figure 1) [28,30–33,37]. The Sanjiang region lies adjacent to the South China block and Songpan-Garzê accretionary complex in the east and the West Burma block in the west [17,30,31]. It is composed of seven blocks, including the Simao block, Baoshan block, Tengchong block, Zhongza block, East Qiangtang block, West Qiangtang block, and Lhasa block (Figure 2). Some sutures are preserved in the Sanjiang region as evidence of the tectonic evolution of the Tethys Ocean, such as Longmucuo-Shuanghu Changning-Menglian, Jinshajiang, Ailaoshan, Garzê-Litang, and Nujiang (Figure 2). Among them, the Longmucuo-Shuanghu suture, Changning-Menglian suture, Jinshajiang suture, and Ailaoshan suture are all north-south sutures (Figure 2) [18,28,30,38–42].

Along with the process of Tethys accretionary orogeny and collisional orogeny, a series of minerals associated with the Tethys orogenic belt developed in the southwestern Sanjiang Tethys orogenic belt. The main mineral types can be divided into eight categories, including volcanogenic massive sulfide (VMS) Pb-Zn-Cu-Ag deposits, porphyry Cu-(Mo-Au) deposits, porphyry Mo-W(-Cu) deposits, magmatic-hydrothermal Sn-W deposits, magmatic-hydrothermal Pb-Zn-Cu-Ag deposits, Mississippi Valley Type (MVT) Pb-Zn deposits, hydrothermal Au deposits and orogenic Au deposits (Figure 1) [17,34]. The porphyry Cu-(Mo-Au) deposits concentrate in the Jinshajiang-Honghe alkali-rich porphyry Cu-(Mo-Au) deposits belt and the Garzê porphyry Cu-(Mo-Au) deposits belt on the southern edge of the Yidun Island arc [43–45]. The mineralization era of the Jinshajiang-Honghe alkali-rich porphyry Cu-(Mo-Au) deposits belt was concentrated in the Cenozoic and can be divided into the Jinshajiang porphyry belt in the north and the Honghe porphyry belt in the south. The porphyry deposits in the North belt are mainly Cu-(Mo-Au) deposits [46–48]. The porphyry deposits in the south belt are mainly Au-(Cu-Mo) deposits [49–52]. The mineralization age of the Garzê porphyry Cu-(Mo-Au) deposits belt on the southern edge of the Yidun Island Arc is Late Triassic [45,53]. Porphyry Mo-W(-Cu) deposits are developed in the southern margin of the Yidun Island Arc of the Sanjiang orogenic belt and the

contact position is between the Garzê–Litang combined zone and the Xiangcheng–Lijiang land margin depression at the western margin of the South China Craton [45,54]. These Late Cretaceous deposits distributed in a nearly north–south direction are large porphyry Mo-W(-Cu) deposits [45,54–56]. The magmatic-hydrothermal Sn-W deposits are located in the Tengchong–Baoshan block, the northern part of the Yidun volcanic arc, and the Changning–Menglian suture. The age span of the deposits ranges from Early Cretaceous, Late Cretaceous, and Paleocene [29,57].

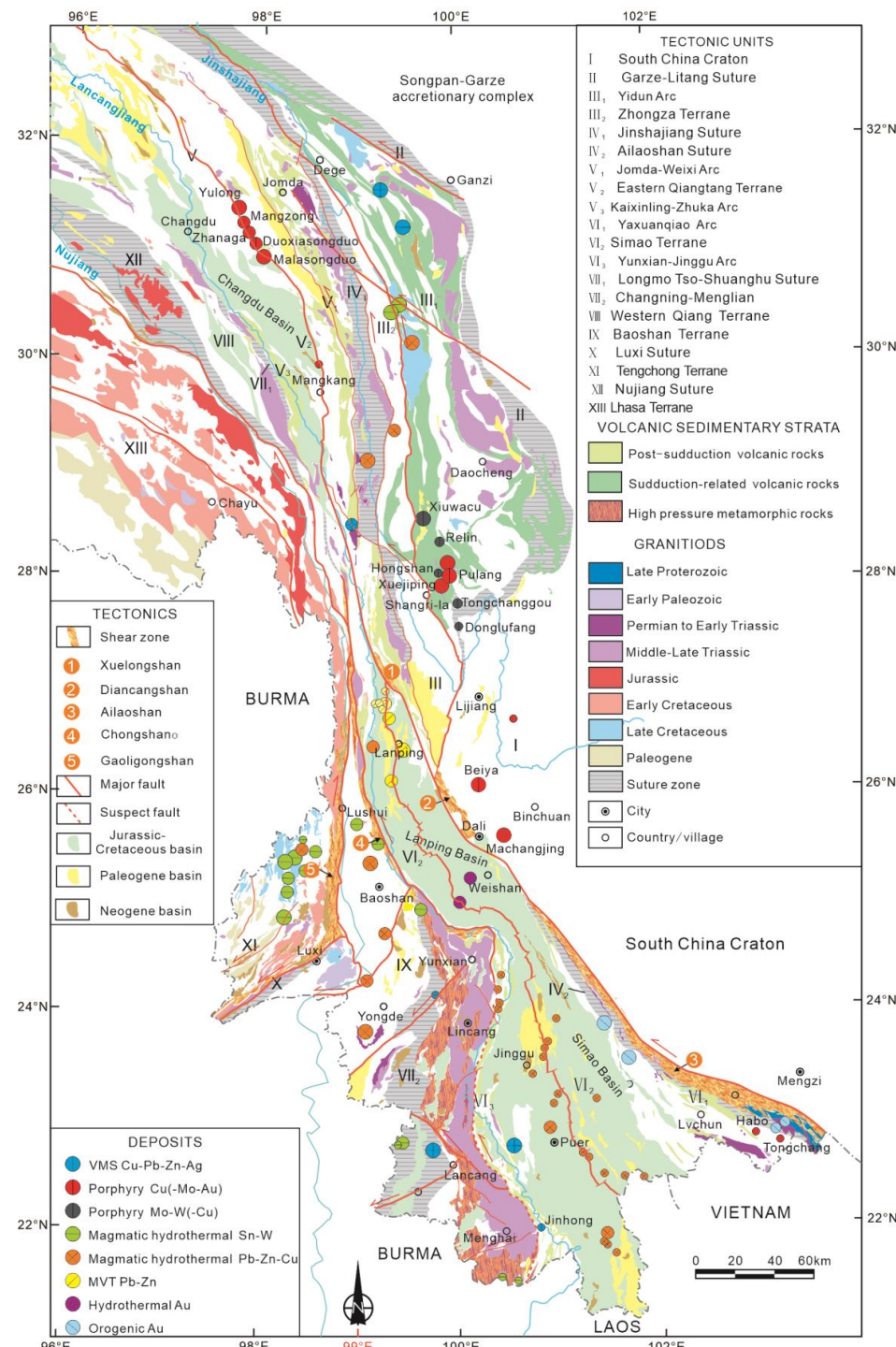


Figure 2. Geological map of the Sanjiang Tethyan Orogen showing the distribution of Early Paleozoic to Cenozoic igneous rocks and major ore deposit. Adapted with permission from Ref. [17]. Copyright 2016 ELSEVIER.

4. Methodology

Among the commonly used isotope systems, the Lu-Hf isotope system has a long half-life and is the most stable in the process of magmatic differentiation [58,59]. Therefore, Lu-Hf isotopes are used for isotopic dating and geochemical tracing. The Lu-Hf isotopic system has been rapidly developed in recent years, and the Hf isotopic signature of magmatic rocks can be used to explore the crustal nature of the magma source area (from ancient or juvenile crust) [60,61]. Three hundred and fifty-nine granitic magmatic rock samples (including 4952 zircon Hf isotope analysis points) were used in combination with existing zircon U-Pb geochronological data to evaluate the crustal evolution in this region through time [38,40,47–49,51,52,62–162]. The samples are mainly neutral-acidic rocks, including quartz diorite, diorite, granite, and granite porphyry. These samples cover almost all of the Sanjiang Tethys except for the Simao block where magmatic rocks are rarely developed. Therefore, the selected samples cover all stages of magmatic activities and can better represent the properties of regional magmatic rocks in the Sanjiang Tethys orogenic belt (Figure 3).

In order to produce a data set that is compatible with the previously published Hf-isotope analyses in the Sanjiang Tethyan Orogen, a consistent method was used to recalculate all of the data, taking a median value from the range of Hf isotopic values of individual samples [17,22,24,163]. The measured $^{176}\text{Lu}/^{177}\text{Hf}$ ratios and a ^{176}Lu decay constant of $1.867 \times 10^{-11} \text{ yr}^{-1}$ were used to calculate the initial $^{176}\text{Hf}/^{177}\text{Hf}$ ratios [164] and the chondritic data of $^{176}\text{Lu}/^{177}\text{Hf} = 0.0336$ and $^{176}\text{Hf}/^{177}\text{Hf} = 0.282785$ were used to calculate the $\epsilon\text{Hf}(t)$ and $f_{\text{Lu/Hf}}$ values [165]. Single-stage model ages (T_{DM}^1) and two-stage model ages (T_{DM}^C) were calculated relative to the depleted mantle values of $(^{176}\text{Hf}/^{177}\text{Hf})_{\text{DM}} = 0.28325$ and $(^{176}\text{Lu}/^{177}\text{Hf})_{\text{DM}} = 0.0384$, a $^{176}\text{Lu}/^{177}\text{Hf}$ ratio of 0.015 was used for the average continental crust, and “ t ” is taken as the crystallization age of the zircon analyzed [166]. The $\epsilon\text{Hf}(t)$, T_{DM} , T_{DM}^C , $f_{\text{Lu/Hf}}$, f_{cc} , f_s , and f_{DM} values were calculated using the formula [164–166]:

$$\begin{aligned} \epsilon\text{Hf}(t) = 10000 \times & \left[\left(\frac{(^{176}\text{Hf}/^{177}\text{Hf})_S - (^{176}\text{Lu}/^{177}\text{Hf})_S \times (e^{\lambda\lambda t} - 1)}{(^{176}\text{Hf}/^{177}\text{Hf})_{\text{CHUR},0} - (^{176}\text{Lu}/^{177}\text{Hf})_{\text{CHUR}} \times (e^{\lambda t} - 1)} \right) - \right. \\ & \left. 1 \right]; T_{\text{DM}} = 1/\lambda \times \ln \left(1 + \left[\frac{(^{176}\text{Hf}/^{177}\text{Hf})_S - (^{176}\text{Hf}/^{177}\text{Hf})_{\text{DM}}}{(^{176}\text{Lu}/^{177}\text{Hf})_S - (^{176}\text{Lu}/^{177}\text{Hf})_{\text{DM}}} \right] \right) / \left[\frac{(^{176}\text{Lu}/^{177}\text{Hf})_S - (^{176}\text{Lu}/^{177}\text{Hf})_{\text{DM}}}{(^{176}\text{Lu}/^{177}\text{Hf})_S} \right]; T_{\text{DM}}^C = T_{\text{DM}} - (T_{\text{DM}} - t) \\ & \times [(f_{\text{cc}} - f_s) / (f_{\text{cc}} - f_{\text{DM}})] f_{\text{Lu/Hf}} = (^{176}\text{Lu}/^{177}\text{Hf})_S / (^{176}\text{Lu}/^{177}\text{Hf})_{\text{CHUR}} - 1, \end{aligned}$$

The Hf contour maps were produced using the inverse distance weighted interpolation methods in the MapGis program to contour the Hf dataset. In order to produce the most robust spatial representation of the isotopic dataset, this method used 12 nearest neighbors at a “power” [16,163].

Since the same sample often has multiple Hf isotope test values, we used the median for a range of Hf isotope values from an individual sample, which helped to exclude abnormal data [17,22,24,163]. The median obtained from the calculation after excluding abnormal data is not affected by the two extremes of maximum and minimum data and can represent the concentrated trend of a set of data, so it can truly reflect the data characteristics of the samples.

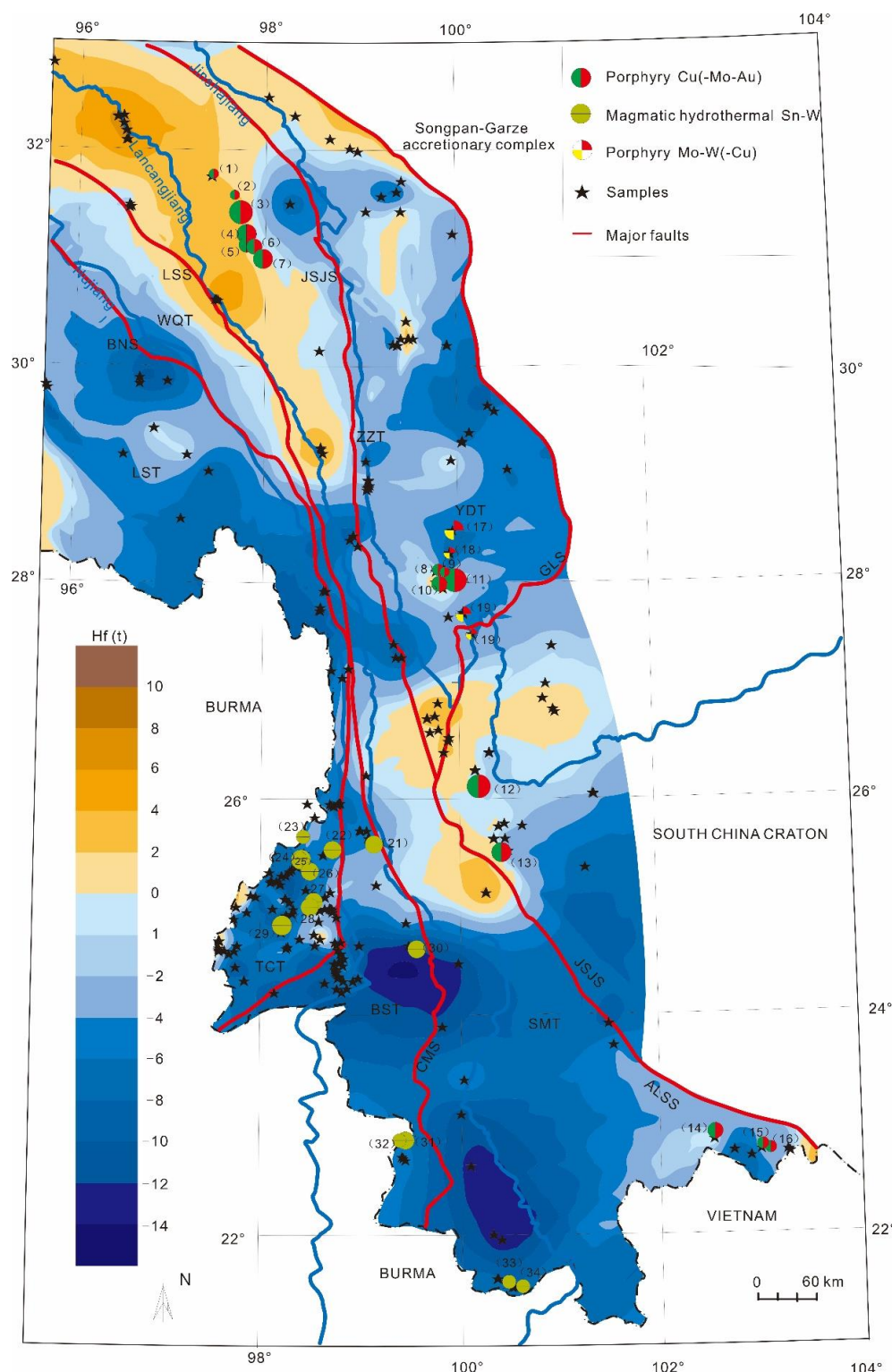


Figure 3. Hf isotopic contour maps showing the spatial variation of zircon ϵHf values for the Early Paleozoic to Cenozoic igneous rocks in the Sanjiang Tethyan Orogen. Abbreviations: BST = Baoshan terrane; EQT = Eastern Qiangtang terrane; LST = Lhasa terrane; SMT = Simao terrane; TCT = Tengchong terrane; WQT = Western Qiangtang terrane; YDT = Yidun arc terrane; ZYT = Zhongza terrane; ALSS = Ailaoshan Suture; BNS = Bangongnu–Nujiang Suture; CMS = Changning–Menglian Suture; JSJS = Jinshajiang Suture; GLS = Garzê–Litang Suture; LSS = Longmucuo–Shuanghu Suture.

5. Results

According to the statistics of zircon $\varepsilon\text{Hf}(t)$ values and the two-stage model age of intermediate acid rocks in Sanjiang Tethys orogenic belt, the $\varepsilon\text{Hf}(t)$ values range from -14 to $+10$, concentrated in the range of -12 to $+8$. The corresponding two-stage model ages range from 0.5 Ga to 2.2 Ga. Zircon $\varepsilon\text{Hf}(t)$ value contours are shown in Figure 3, where the warm color system is for positive $\varepsilon\text{Hf}(t)$ values, and the darker the color the larger the positive value. The cold color system is for negative $\varepsilon\text{Hf}(t)$ values, and the darker the color the smaller the negative value.

The contour results show that there are several anomalous regions with high $\varepsilon\text{Hf}(t)$ values in the Sanjiang Tethys orogenic belt (Figure 3). The anomalous areas with high $\varepsilon\text{Hf}(t)$ values are distributed roughly along the Jinshajiang–Ailaoshan suture on both sides and mainly occur in the East Qiangtang block that belongs to the northern part of the suture ($\varepsilon\text{Hf}(t) = 3.3$; $T_{\text{DM}}^c = 0.9$ Ma), the Yidun Island arc that belongs to the central part of the suture ($\varepsilon\text{Hf}(t) = 1.1$; $T_{\text{DM}}^c = 1.2$ Ga), a small part of the Simao block that belongs to the southern part of the suture ($\varepsilon\text{Hf}(t) = 4$; $T_{\text{DM}}^c = 0.8$ Ga), and the southern part of the South China Craton ($\varepsilon\text{Hf}(t) = 4$; $T_{\text{DM}}^c = 1.0$ Ga). High εHf values are also present at the eastern margin of the Lhasa block, the eastern margin of the Tengchong block, and the southern margin of the Ailaoshan suture on a local scale.

The contour results also show several low εHf value anomalous regions (Figure 3). The low εHf anomalies are located in the Tengchong–Baoshan block ($\varepsilon\text{Hf}(t) = -6.5$), both sides of the Changning–Menglian suture ($\varepsilon\text{Hf}(t) = -11.4$), and the Zhongzhan block ($\varepsilon\text{Hf}(t) = -6.5$). It is worth noting that the Simao block magmatic rocks are shown as negative $\varepsilon\text{Hf}(t)$ anomalies in the figure due to the lack of sufficient research data, which are influenced by the surrounding values.

Meanwhile, the contour results also show that all porphyry Cu(-Mo-Au) deposits (e.g., Yulong porphyry ore field (No. 1–7) in the northern segment, the Beiya (No. 12) and Machangqing (No. 13) ore deposits in the central, and the Habo (No. 14) and Tongchang (No. 16) ore deposits in the southern) are located in the high $\varepsilon\text{Hf}(t)$ region ($\varepsilon\text{Hf}(t) > 0$). Porphyry Mo-W(-Cu) deposits (e.g., Xiuwacu (No. 17), Relin (No. 18), Donglufang (No. 20)) and Magmatic hydrothermal Sn-W deposits (e.g., Xiaolonghe (No. 24) and Lailishan (No. 29)) are strictly restricted to the low $\varepsilon\text{Hf}(t)$ region ($\varepsilon\text{Hf}(t) < 0$) (Figures 3 and 4, Table 1).

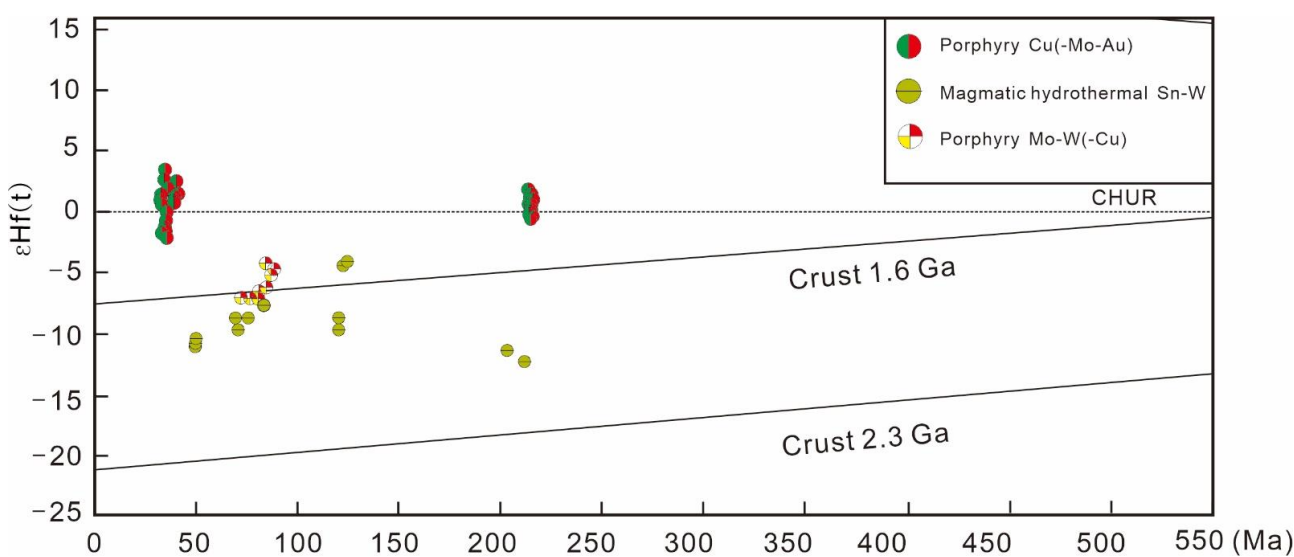


Figure 4. Plots of median $\varepsilon\text{Hf}(t)$ versus U-Pb ages of magmatic zircons.

Table 1. A summary of the geological characteristics of major ore deposits in the Sanjiang Tethyan Orogen.

Deposit	Long./Lat.	Type	Mineral Element	Tonnage	Grade (%)	Host Rock	Alteration	Igneous Age (Ma)	Mineralization Age (Ma) Molybdenite Re-Os	$\epsilon_{\text{Hf}} (\text{t})$	Data Source
Baomai (1)	97.43/ 31.77	Porphyry	Cu-Mo	Cu:0.21 Mt Mo:0.06 Mt	Cu:0.22% Mo:0.06%	Biotite granite, biotite monzogranite	Potassic, propylitic, phyllitic, argillic and skar	LA-ICP-MS zircon U-Pb: 37.8 ± 0.2; 42.7 ± 0.2	42.6 ± 0.3	-0.4~4.9	[47]
Hengxingcuo (2)	97.71/ 31.51	Porphyry	Cu-Mo	No data	No data	granite porphyry;	No data	No data	No data	No data	[167]
Yulong (3)	97.72/ 31.42	Porphyry	Cu-Mo-Au	Cu:6.22 Mt Mo:0.06 Mt	Cu:0.99% Mo:0.28% Au:0.35 g/t	Biotite monzogranite, granodiorite, alkali-feldspar granite	Potassic, propylitic, phyllitic, argillic and skarn	LA-ICP-MS zircon U-Pb: 41.2 ± 0.2; SHRIMP zircon U-Pb: 40.9 ± 0.1	40.1 ± 1.8; 41.6 ± 1.4	-0.2~4.3	[46,47,153,168,169]
Zhanaga (4)	97.79/ 31.23	Porphyry	Cu-Mo-Au	Cu:0.3 Mt	Cu:0.36% Mo:0.03% Au:0.03 g/t	Monzogranite, syenogranite	Potassic, phyllitic, argillic, propylitic	SHRIMP zircon U-Pb: 38.5 ± 0.2	No data	1.5~4.3	[46,168,169]
Mangzong (5)	97.79/ 31.13	Porphyry	Cu-Mo-Au	Cu:0.25 Mt	Cu:0.34% Mo:0.03% Au:0.02 g/t	Monzogranite	Potassic, phyllitic, propylitic	LA-ICP-MS zircon U-Pb: 37.6 ± 0.2	No data	No data	[46,168,169]
Duoxiasongduo (6)	97.88/ 31.11	Porphyry	Cu-Mo-Au	Cu:0.5 Mt	Cu:0.38% Mo:0.04% Au:0.05 g/t	Monzogranite, granite, syenogranite	potassic, phyllitic, propylitic	SHRIMP zircon U-Pb: 37.5 ± 0.2	36 ± 0.4	No data	[46,168,169]
Malasongduo (7)	97.97/ 30.99	Porphyry	Cu-Mo-Au	Cu:100 Mt	Cu:0.44% Mo:0.14% Au:0.06 g/t	Alkali-feldspar granite	Potassic, phyllitic and argillic	LA-ICP-MS zircon U-Pb: 36.9 ± 0.4	35.8 ± 0.4	No data	[46,168,169]
Lannitang (8)	99.82/ 28.14	Porphyry	Cu-Au	Cu:36 Mt	Cu:0.50%, Au:0.45 g/t	Quartz monzonite porphyry Diorite porphyrite	Potassic alteration, quartz sericitization and argillization	LA-ICP-MS zircon U-Pb: 225.2 ± 3.5	No data	-1.1~0.6	[55,122,170]
Honhshan (9)	99.88/ 28.12	Porphyry	Cu-Mo	Cu:65 Mt Mo:0.58 Mt	Cu:1.23% Mo:0.14%	Quartz monzonite porphyry	Skarnization	LA-ICPMS zircon U-Pb: 75.8 ± 1.3	77.9 ± 1.1; 81.05 ± 1.17	-8.8~5.5	[72,73,122,156]
Xuejiping (10)	99.83/ 28.01	Porphyry	Cu-Au	Cu:54.15 Mt	Cu:0.53% Au:0.06 g/t	Dioritic porphyry and monzonitic	Potassic alteration and quartz sericit	SIMS zircon U-Pb: 218.3 ± 1.6; 218.5 ± 1.6,	221.4 ± 1.3	-2.7~4.4	[55,82,100,122]
Pulang (11)	99.99/ 28.04	Porphyry	Cu-Mo-Au	Cu:1625 Mt; Mo:84.8 Kt; Au:28.8 t	Cu:0.52%; Mo:0.004%; Au:0.18 g/t	Quartz diorite porphyry, quartz monzonite porphyry	Potassic alteration silification	MS zircon U-Pb: 221.0 ± 1.0; 211.8 ± 0.5,	218 ± 3.4; 219.7 ± 3.4	-2.4~2	[55,122,159,171]
Beiya (12)	100.22/ 26.14	Porphyry	Cu-Au-Fe	Cu:0.26 Mt; Au:127 t; Fe:30 Mt	Cu:0.5%; Au:2.45 g/t; Fe:35%	Quartz-albite porphyry, quartz porphyry, biotite-K-feldspar porphyry,	Potassic alteration, silification, sericitization, chloritization, carbonization	LA-ICP-MS zircon U-Pb: 34.72 ± 0.94; 37.67 ± 0.97	36.82 ± 0.5	-4.5~4.3	[48,49]

Table 1. Cont.

Deposit	Long./Lat.	Type	Mineral Elemen	Tonnage	Grade (%)	Host Rock	Alteration	Igneous Age (Ma)	Mineralization Age (Ma) Molybdenite Re-Os	ε Hf (t)	Data Source
Machangqing (13)	100.44/ 25.53	Porphyry	Cu-Mo-Au	Cu:81,258 t; Mo:44,525 t; Au:26 t	Cu:0.50%; Mo:0.08%; Au:4.01–8.70 g/t	Syenite porphyry; monzonite porphyry; granite porphyry; limestone and sandstone	Potassic alteration, silicification, sericitization chloritization,	LA-ICP-MS zircon U-Pb: 33.78 ± 0.21; 35.6 ± 0.3; 35.0 ± 0.2; 37.93 ± 0.82	35.3 ± 0.7; 35.8 ± 1.6; 33.9 ± 1.1; 34.72 ± 0.5	-2.4~1.2	[50,172]
Habo (14)	102.54/ 22.94	Porphyry	Cu-Mo-Au	Cu:0.53 Mt Mo:37718 t	Cu:0.42– 1% Mo:0.01–0.1% Au:1–33 g/t	Biotite quartz monzogranite; quartz monzonite porphyry; monzonite porphyry	K-silicate, quartz- sericite, propylitic	LA-ICP-MS zircon U-Pb: 36.34 ± 0.63; 35.99 ± 0.36	35.47 ± 0.2	-4.3~−1.1	[51]
Chang'anchong (15)	103.01/ 22.81	Porphyry	Cu-Mo-Au	Cu:29,337 t Mo:13,310 t	Cu:1.48% Mo:0.13% Au:0.25 g/t	Quartz monzonite granite	K-silicate, quartz- sericite, skarn	LA-ICP-MS zircon U-Pb: 36.3 ± 0.3; 33.7 ± 0.8	34.54 ± 0.7	No data	[172]
Tongchang (16)	103.05/ 22.79	Porphyry	Cu-Mo-Au	Cu:0.01 Mt Mo:0.02 Mt	Cu:1.24% Mo:0.218% Au:0.13 g/t	Quartz syenite porphyry	K-silicate, quartz- sericite, skarn	LA-ICP-MS zircon U-Pb: 34.6 ± 0.2; 35.1 ± 0.3	34.38 ± 0.5; 34.2 ± 0.3	-4.4~−1.2	[172]
Xiuwacu (17)	99.99/ 28.5	Porphyry	Mo-W	Mo:1.36 Mt WO ₃ :0.84 Mt	Mo:0.38% WO ₃ :0.28%	Biotite monzogranite, alkali-feldspar granite	Propylitization, potassic alteration and sericitization	LA-ICPMS zircon U-Pb: 85.6 ± 0.5; 84.8 ± 0.6; 84.4 ± 1.4	82.3 ± 1.1; 83.5 ± 0.3	-7.1~−3.6	[55,72,73]
Relin (18)	99.94/ 28.29	Porphyry	Mo-Cu		Mo:0.049%	Monzogranite, granite porphyry	Propylitization, potassic alteration and skarnization	LA-ICPMS zircon U-Pb: 82.7 ± 0.5	80.3 ± 1.1; 82.9 ± 1.1	-9.0~−4.6	[55,72,73]
Tongchanggou (19)	100.08/ 27.23	Porphyry-skarn	Mo-Cu	Mo:30 Mt Cu:0.34 Mt	Mo:0.3% Cu:0.8%	Granodiorite porphyry		LA-ICP-MS zircon U-Pb: 85.7 ± 0.5; 84.7 ± 0.6	86.8 ± 0.6; 85.2 ± 0.4	-5.7~−2.7	[73,157]
Donglufang (20)	100.16/ 27.54	Porphyry	Mo-Cu	80 Mt	Mo:0.15% Cu:0.48%	granodiorite porphyry	Potassic, propylitic, phyllitic, argillic and skarn	LA-ICP-MS zircon U-Pb: 85.1 ± 0.5; 84.4.1 ± 0.3	84.9 ± 1.0	-9.9~−0.5	[143]
Tiechang (21)	99.15/ 25.58	Hydrothermal type	Sn-W	No data	Sn:1.22%	granite, gneiss	Sericitization, silicification, chloritization	No data	No data	No data	[17,57]
Dadongchang (22)	98.73/ 25.53	Hydrothermal type	Sn	Sn:10,000 Mt	Sn:0.14%; Pb:8.18%; Zn:18.0%; Cu:0.73	biotite granite, dolomitic, limestone, arenaceous mudstone and sandstone	Skarnization, silicification, tremolitization, sericitization, chloritization, fluoritization	Early Cretaceous	118.0 ± 2.4	No data	[17,57]

Table 1. *Cont.*

Deposit	Long./Lat.	Type	Mineral Elemen	Tonnage	Grade (%)	Host Rock	Alteration	Igneous Age (Ma)	Mineralization Age (Ma) Molybdenite Re-Os	ε Hf (t)	Data Source
Diantan (23)	98.43/ 25.65	Hydrothermal type	Sn–Fe	No data	No data	alkali feldspar granite, dolomitic limestone, mudstone and sandstone	Skarnization, silicification, sericitization, chloritization	LA-ICP-MS zircon U-Pb: 122.0 \pm 2.1; 123.0 \pm 1.4	No data	-3.9~−4.0	[17,57,106]
Xiaolonghe (24)	98.41/ 25.44	Hydrothermal type	Sn	Sn:26,200	Sn:0.18–0.42%	biotite granite, sandy slate	Greisenization, sericitization, silicification, chloritization	LA-ICP-MS zircon U-Pb: 75.2 \pm 4.2; 70.5 \pm 3.4	No data	-11.3~−1.7	[17,87,106,115]
Dasongpo (25)	98.4/ 25.45	Hydrothermal type	Sn	Sn:>1000	Sn:1.38%	biotite granite and monzogranite, sandy slate	Greisenization, sericitization, silicification, chloritization	LA-ICP-MS zircon U-Pb: 70.3 \pm 3.2; 71.5 \pm 2.1	No data	-8.4~−5.0	[17,106]
Gudong (26)	98.5/ 25.33	Hydrothermal type	Sn	No data	No data	biotite granite, sandy slate	Greisenization, sericitization, silicification, chloritization	No data	No data	No data	[17]
Baihuanao (27)	98.54/25.05	Hydrothermal type	Sn	Sn:12,638	Sn:0.014%	biotite albite granite	Albitization, greisenization, amazonization	LA-ICP-MS zircon U-Pb: 61.9 \pm 1.4	No data	-11.8~−8.5	[17,87]
Xinqi (28)	98.50/ 25.00	Hydrothermal type	Sn	No data	Sn:0.47%	monzogranite, schist, leptynite	Greisenization, silicification, sericitization,	LA-ICP-MS zircon U-Pb: 61.9 \pm 1.4	No data	No data	[17]
Lailishan (29)	98.22/ 24.83	Hydrothermal type	Sn	Sn:42,600	Sn:1.11%	biotite granite, monzogranite, and feldspar granite; sandstone and slate	Potassic alteration kaolinization, sericitization, silicification, chloritization	LA-ICP-MS zircon U-Pb: 45.77 \pm 0.89; 50.0 \pm 1.6	No data	-11.9~−8.0	[17,93,115]
Haobadi (30)	99.58/ 24.61	Hydrothermal type	Sn	Sn:8600	Sn:0.95%	monzogranite, sandstone, quartz sandstone, quartzite	Silicification	LA-ICP-MS Zircon U-Pb: 231.5 \pm 3.6	No data	No data	[17,57]
A'mo (31)	99.46/ 22.84	Hydrothermal type	Sn	No data	Sn:1.07%	biotite granite, two-mica granite, and pegmatite, marble, schist	Albitization	No data	Taeniolite Rb-Sr age, 21.5	No data	[17,57]
Damasa (32)	99.40/ 22.84	Hydrothermal type	Sn	No data	No data	biotite granite	No data	No data	No data	No data	[17,57]
Bulangshan (33)	100.45/ 21.43	Hydrothermal type	Sn	No data	No data	granite	Albitization, tourmalinization, silicification, greisenization	LA-ICP-MS zircon U-Pb: 216 \pm 1; 218 \pm 1	No data	-10.8~−7.4	[17,57,160]
Mengsong (34)	100.54/ 21.38	Hydrothermal type	Sn	No data	No data	granite	Albitization, tourmalinization, silicification, greisenization	LA-ICP-MS zircon U-Pb: 228 \pm 2; 222 \pm 1,	No data	-14.4~−10.1	[17,57,160]

6. Discussion

6.1. Distribution of Different Deposits Constrained from Zircon Hf-Isotopic Mapping

Previous knowledge of the lithospheric structure and deep tectonic framework of the Sanjiang Tethys orogenic belt was mainly speculated by geophysical means [37,173] but lacked material information support. Neutral-acid rocks are widely developed in the Sanjiang Tethys orogenic belt. These zircon Hf isotopes can be used as a “rock probe” to trace the petrogenesis, so as to reflect the material composition and temporal and spatial changes in different parts of the crust. In this study, based on the contour map of granitic zircon $\epsilon\text{Hf(t)}$ values, we can demonstrate the spatial distribution and spatial transformation of the model ages of deep source rocks in the crust, and thus determine the spatial distribution and temporal evolution of different terranes.

Zircon Hf isotope mapping shows that there are widespread negative $\epsilon\text{Hf(t)}$ values in the Tengchong block, Baoshan block, and Changning–Menglian suture in the west of Sanjiang Tethys orogenic belt and Zhongzan block Yidun island arc belt in the east, which correspond to two-stage model ages $T_{\text{DM}}^{\text{c}} > 1.2 \text{ Ga}$, suggesting that these terranes may be ancient, locally modified crustal blocks. Spatially, the higher $\epsilon\text{Hf(t)}$ values correspond to a younger T_{DM}^{c} age in the east Qiangtang block, the southern part of the Yidun Island arc, the Simao block, and the southern margin of the South China Craton, which are located in the eastern part of the Sanjiang Tethys orogenic belt, indicating that the petrogenesis of these regions is dominated by newly formed mantle-derived components.

Combining Hf isotope mapping results with geophysical exploration, we can construct a three-dimensional lithospheric structure at the scale of the terrane. Zhou [37] speculated that the crust of the southwest Sanjiang Tethys orogenic belt shows a “stepwise” thickening trend from west to east and from south to north. The 3D model map from the terrane to the South China Craton shows that the Tengchong–Baoshan block has an approximately 35 km thick crust with negative $\epsilon\text{Hf(t)}$ values and old model ages (T_{DM}^{c} values), indicating the presence of older crustal components and remelted crustal components in the magmatic rocks of the region [17,34]. In contrast, the continental crust of the eastern South China Craton is about 45 km thick and the magmatic zircons have positive $\epsilon\text{Hf(t)}$ values and young model ages (T_{DM}^{c} values), indicating the incorporation of juvenile mantle-derived material in the magma source area of the region [17,34].

Therefore, based on zircon Hf isotope regional mapping, the Sanjiang region shows temporal and spatial heterogeneity of the crust, which is bounded by the Longmucuo–Shuanghu suture and the Changning–Menglian suture. The ancient crust of negative $\epsilon\text{Hf(t)}$ values is mainly in the west and the juvenile crust of positive $\epsilon\text{Hf(t)}$ values is mainly in the east.

The zircon Hf isotope mapping of granitic rocks in the Sanjiang region reveals that the mineralization system in the Sanjiang region is controlled by the crustal properties in the region, and the differences in crustal properties constrain the distribution pattern of different mineralizing elements (Figure 3). The results of zircon Hf isotope mapping prove that the properties and composition of the crust are closely related to the formation and spatial distribution of polymetallic deposits. Firstly, all porphyry Cu-(Mo-Au) are located within the juvenile crustal blocks with high ϵHf values. This is consistent with the Cu-ore-forming magmas in the Jinshajiang–Ailaoshan suture mainly sourced from the juvenile lower crust [94]. Secondly, all magmatic-hydrothermal Sn-W deposits and porphyry Mo-W(-Cu) deposits are strictly controlled by the reworking of an ancient crust with negative ϵHf values and are mainly distributed in the Tengchong block, the Yidun island arc, and the Changning–Menglian suture (Figures 3 and 4).

6.2. Exploration for the Sanjiang Tethyan Orogenic Belt

The Triassic porphyry Cu(-Mo-Au) deposits and Middle Eocene to Early Oligocene porphyry Cu(-Mo-Au) deposits are developed in a magmatic arc within the Garzê–Litang suture and the Jinshajiang–Laohuoshan suture zone, with a high $\epsilon\text{Hf(t)}$ region (Figures 3 and 4). Ore-bearing porphyry magmas forming the juvenile lower crust in the Sanjiang Tethyan orogenic belt were derived from asthenospheric mantle wedge metasomatized by the

upwelling of the asthenosphere in post-subduction and post-collision settings [17]. The underplating of these magmas at the bottom of the crust inevitably led to the enrichment of the juvenile lower crust in Cu(-Mo-Au) contents (Figure 5) [16]. These results suggest that the juvenile crust plays a major controlling role in the formation of porphyry Cu(-Mo-Au) deposits.

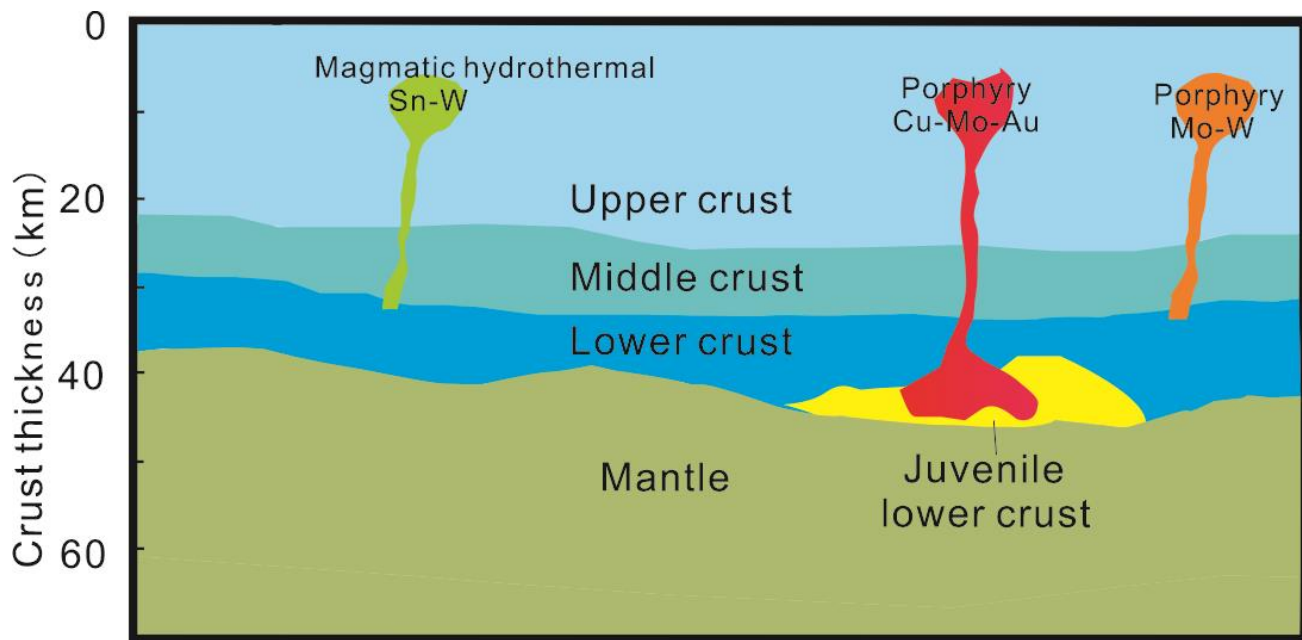


Figure 5. Model of composite metallogenetic systems.

Late Triassic I-type granites and related porphyry Cu–Mo deposits (e.g., Xuejiping (No. 10), Pulang (No. 11)) occur in the southern part of the Yidun Arc (Figure 3 and Table 1). The porphyry Cu mineralization in the southern part of the Yidun Arc region most likely originated from the enriched mantle wedge metasomatized by subduction-derived fluids and sediments [55,174]. The subduction-derived fluids and sediments not only provided the volatile components (H_2O and Cl) but also controlled the high oxygen fugacity (f_{O_2}), which makes calc-alkaline magmas favorable for porphyry Cu mineralization [55,174].

A small area of high $\epsilon Hf(t)$ anomaly is distributed in the Yidun Island Arc, mainly located at the southern margin of the Yidun Arc. The area reveals medium acidic volcanic rocks of the Upper Triassic Tumgou Formation interspersed with shallow metamorphic sandy mudstone and carbonate rock stratigraphy [45,55]. In general, it is an NW-trending compound anticline structure that developed NW-trending faults [55,175]. The medium acidic (porphyritic) rocks are widely distributed in groups, which can be divided into three rock belts from east to west: the Late Triassic island arc porphyry belt in the eastern north, the Early Triassic genus ophiolitic melange belt in the middle, and the Early and Middle Triassic porphyry belts in the southwest [53]. This area is located in the North-South positive magnetic anomaly zone, and both sides are gentle negative magnetic field areas. Regional chemical prospecting has identified several “high, large, and complete” anomalies with high intensity, large lining, large scale, good concentration zoning, and obvious concentration centers, such as Cu, Mo, Pb, Zn, Ag, and Au [53]. The remote sensing image shows a dense intersection of northwest and northeast linear tectonics, forming a fine rhombic network of fracture blocks, with magma rings and hydrothermal rings developed in complex combinations of overlapping, concentric, and offset superposition [53,175]. Important porphyry Cu(-Mo-Au) deposits such as Pulang (No. 11) ultra-large porphyry, Xuejiping (No. 10), and Hongshan (No. 9) have been evaluated in this area [45,55,171,176], and its periphery, Pushang and Songnuo, have a similar metallogenetic background and mineralization characteristics as Pulang. It is a favorable area for finding porphyry Cu(-Mo-Au)

deposits, and the prospecting prospect is good [53], which is consistent with the area with a high abnormal value of Hf in this paper.

Middle Eocene to Early Oligocene potassic–ultrapotassic intrusive rocks and related porphyry Cu–Mo–Au deposits dominantly extend along the Jinshajiang–Ailaoshan tectonic belt [30,33]. The potassic–ultrapotassic intrusive rocks are derived from the partial melting of a thickened, potassic, mafic lower crust with minor input from an older igneous felsic component. Partial melts of K-rich mafic lower crust produced high-K calc-alkaline granitic intrusions and porphyry Cu–Mo deposits [94].

The high $\epsilon\text{Hf(t)}$ anomaly region in the northern part of the Jinshajiang–Ailaoshan suture is between the Jinshajiang binding zone and the Nujiang binding zone. In between, the Jinshajiang basal–ultramafic zone, Baimaxueshan granite belt, Yulong alkaline granite belt, the Leiwuqi–Dongdashedan granite zone, Nujiang–Bitu basic ultrabasic rock belt, Guoqingchaw granite belt, and Zaxize–Sanmiancun granite belt are developed from east to west [53]. The geochemical anomalies in this area are controlled by regional geological structure and magmatic rocks and are distributed in the NW–SE direction. From east to west, it can be clearly divided into four anomalous zones: Jinshajiang Au and Cu polymetallic anomalous zone; Yulong porphyry Cu and Mo anomalous zone; Lancangjiang W, Sn, Pb, Zn, Ag, Cu polymetallic anomalous zone; and Nujiang Au, Pb, Ag, W, Sn, Cu polymetallic anomalous zone [53]. The discovered and evaluated large and medium-sized porphyry Cu(-Mo-Au) deposits are all produced in the banded Yulong porphyry Cu and Mo anomaly, which is consistent with the high $\epsilon\text{Hf(t)}$ anomaly area. In addition, the distribution characteristics of the enrichment degree and dispersion of elements in the earth rocks and aqueous sediments of the eastern Tibetan region suggest that the eastern Tibetan earth has very good prospects for polymetallic mineralization such as Cu–Mo, Au, Pb, and Zn [53,177], which is consistent with the region of high anomalous values of Hf in this paper.

A high $\epsilon\text{Hf(t)}$ anomaly region is also seen in the south-central part of the Jinshajiang–Ailaoshan suture. This anomalous region is consistent with the distribution of the Himalayan alkali-rich porphyry belt in western Yunnan. The alkali-rich porphyry belt in western Yunnan can be divided from north to south into six alkali-rich porphyry groups: the Bengge–Taohua Group, the Yongsheng–Ninglang Group, the Machangqing–Beiya–Liuhe Group, the Yongping–Weishan Group, the Yaoan–Huaping Group, and the Jinping–Luchun Group (Figure 6) [178,179]. The quartz diorite porphyry and quartz diorite porphyrites in the contact zone of the Jinsichang and Taohua areas (Figure 6) are commonly developed with strong silicification, hornification, yellow (brown) iron mineralization, and skarnization. Large-scale physical surveys in the Taohua–Jinsichang area also show the existence of concealed ore bodies and concealed rock bodies and the presence of chemical anomalies of Cu, Pb, Zn, Ag, Au, Sb, and other elements [50]. In the area of Ninglang–Yongsheng (Figure 6), 47 gold anomalies were traced by the chemical anomalies, which were distributed in the NE direction and coincided with the Cu anomalies. The Cu anomaly is accompanied by the main fracture in a band-like spreading, forming a concentration center with $w(\text{Cu}) > 300 \times 10^{-6}$ in the Bainiuchang and Luobodi areas, generally containing $w(\text{Au})$ of $(5\sim7) \times 10^{-9}$ and $w(\text{Ag})$ of $(0.15\sim1.2) \times 10^{-6}$ [53]. The Beiya and Heqing (Figure 6) areas are dominated by chemical anomalies of gold, with a large scale, high intensity, and obvious concentration center. Important gold anomalies include Songgui, Tanyao, Beiya, and Huadianba. In the Tiesuodongshan area of Yongren, Yunnan, the geochemical anomalies are mainly Cu, Pb, Au, Pb, Ag, and Mo, among which the copper anomalies mostly coincide with the Cu deposits in the area, and some of the gold-copper anomalies are located in the distribution area of porphyry bodies or their sides [53]. In the Weishan–Yongping area (Figure 6), regional chemical probes show Au, Sb, Hg, As, Cu, Co, Pb, Zn, Ag, and other elemental anomalies [180]. Au anomaly higher values are mainly located in Yongping Zhuopan, Yangbi Huanglianpu, Weishan Zijinshan, Weishan Lianhuashan, and Nanrun Gonglanghu areas [180]. The higher value of Cu anomalies is mainly concentrated in Yongpingchang Street, Shuixie, and Nanjian Gonglanghu areas,

and the Co anomaly is basically similar to the Cu anomaly [180]. West Yunnan has a large distribution of Himalayan copper-bearing porphyry bodies, and porphyry alteration and strong Cu mineralization are commonly seen. It is a favorable area for exploring porphyry Cu(-Mo-Au) deposits.

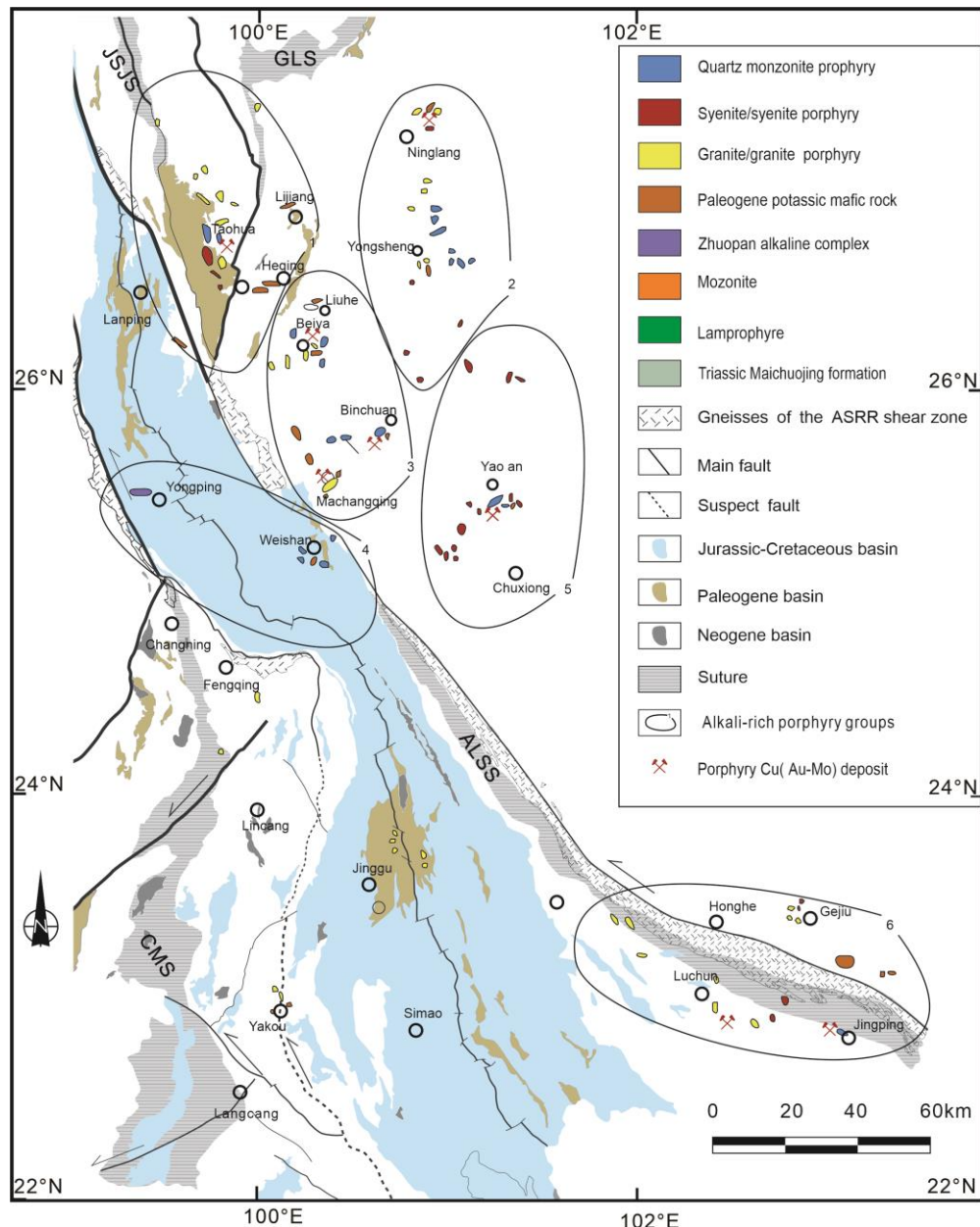


Figure 6. Cenozoic alkali-rich porphyry showing distribution in western Yunnan. Adapted with permission from Ref. [152]. Copyright 2020 Wiley Online Library.

The spatial distribution of porphyry Mo-W(-Cu) deposits and magmatic hydrothermal Sn-W deposits are strictly restricted to the low $\epsilon\text{Hf(t)}$ region (Figure 3). Proven porphyry Mo-W(-Cu) deposits (Xiuwacu (No. 17), Relin (No. 18), Tongchanggou (No. 19), and Donglufang (No. 20)) are concentrated at the edge of reworked old crust or near the ancient crust. Similarly, the identified Magmatic hydrothermal Sn-W deposits (Xiaolonghe (No. 24), Dasongpo (No. 25), Lailishan (No. 29)) are concentrated in the ancient T_{DM}^{c} crustal zone or developed along the $\epsilon\text{Hf(t)}$ value isotopic boundary of ancient crustal blocks. These features suggest that the spatial distribution of Sn-W and Mo-W deposits is closely related

to the compositional heterogeneity and remelting/modification of ancient crustal blocks (Figure 5).

Late Cretaceous magmatic rocks are developed in Xiuwacu, Relin, Donglufang, and other areas on the southern margin of the Yidun Island Arc (Figure 2). The magmatic activity in this period is that the Yidun Island Arc is in the extensional background, due to the thinning of the lithosphere. The asthenosphere material upwelled, the temperature of the lower part of the rock group increased, and the thickened lower crust was partially melted [55]. During the partial melting of the lower crust, chalcophile elements (such as Cu) were removed, but siderophile metals (such as Mo) were left as a residue in the cumulate zone of the deep arc crust and/or in the metasomatized mantle lithosphere. This mechanism facilitated porphyry Mo-Cu mineralization in the southern Yidun Terrane (Figure 5) [156]. Elemental and chemical anomalies of Mo, W, Sn, and Bi in the Yidun Island arc region are mainly distributed in the Xiuwacu, Yaza-Lantang-Pulang, and Gelu areas of the Garzê porphyry belt [56]. Among them, the Mo, W, Sn, and Bi anomalies located in the Xiuwacu promotion site are large in scale, high in intensity, and obvious in concentration centers, with tertiary concentration zoning, representing the strong Mo-W mineralization in the area [56]. These areas of chemical anomalies are generally consistent with the transformation sites of the low $\epsilon\text{Hf(t)}$ isotope anomalies in zircon.

The western Yunnan Sn belt is mainly developed in the Teng-Liang area, Baoshan block, Changning-Menglian, and Lincang combined belt, all in the region of low zircon $\epsilon\text{Hf(t)}$ values. The Sn bearing granites in western Yunnan can be divided into three granite belts: Yunlong-Mengnan (East Asian belt), Changning-Ximeng (Central Asian belt), and Tengchong-Lianghe (West Asian belt) [181]. The comparative research revealed that the Sn-bearing granite belt in western Yunnan belongs to the northern extension of the Sn-bearing granite belt in Southeast Asia [182]. The Sn-bearing granites are produced by regional tectonics driven by micro-plate subduction and collision [115]. At present, most of the discovered deposits in the Sn belt in western Yunnan are related to the remodeling-remelting granite magmatic activity [115]. The remodeling-remelting of the crust enriches the metallogenic metal elements initially dispersed in the crust (mantle). Regional geochemical studies show that Sn polymetallic deposits in western Yunnan are mainly located in the low-gravity anomaly zone ($-2 \text{ mGal} \sim -10 \text{ mGal}$), and the range of weak positive aeromagnetic anomalies ($0 \text{--} 100 \text{ nT}$) reflects that the Sn polymetallic deposits in western Yunnan are mainly associated with granites and sedimentary rocks [115]. Regional chemical anomalies from east to west can be divided into the Tengchong Sn polymetallic anomaly; the Gaoligongshan-Longchuan Sn, W, Be, Nb anomaly; the Luxi Sn, W, Be anomaly; and the Changning-Ximeng Sn, B anomaly [183]. Large and medium-sized deposits such as Lailishan and Xiaolonghe have been discovered in these anomalous zones.

The crustal structure constrains the formation of metallogenic systems and the spatial distribution of mineral deposits. Therefore, zircon Hf isotope mapping can be used as a method to constrain regional mineralization targets by combining regional geological features and geophysical and geochemical anomalies. The northern part of the East Qiangtang region, the central part of the Jinshajiang-Ailaoshan suture, the southern extension of the Ailaoshan suture, and the Vietnam region, which show high $\epsilon\text{Hf(t)}$ anomalies, may have prospective areas for porphyry Cu(-Mo-Au) deposits. In parts of the Tengchong-Baoshan block—that is, the anomaly with low $\epsilon\text{Hf(t)}$ —there may be promising areas of Magmatic hydrothermal Sn-W deposits. The southern edge of the Yidun Island Arc, the transformation site of the zircon $\epsilon\text{Hf(t)}$ isotope anomaly, has the potential to host prospective porphyry Mo-W(-Cu) deposits.

7. Conclusions

Through the Hf isotope mapping of granite-like zircon in the Sanjiang area, the properties and components of the crust in the Sanjiang area are revealed. It was concluded that the eastern part of the crust is dominated by the juvenile crust and the western part by the ancient crust. Meanwhile, from the Hf isotope mapping of granite-like zircon in

the Sanjiang area, it is deduced that the lithospheric structure and its crustal type are the first-order factors that constrain the distribution of different minerals. Zircon Hf isotope regional mapping, combined with regional geological features, geophysical anomalies, and geochemical anomalies, can be used to predict regional mineralization. The northern part of the East Qiangtang area, the central part of the Jinsha River–Ailaoshan suture, the southern extension of the Ailaoshan area, and the Vietnam area may become the most potential porphyry Cu(-Mo-Au) metallogenic areas. There are potential areas for magmatic hydrothermal Sn-W deposits in some areas of the Tengchong–Baoshan block. The southern margin of the Yidun Island Arc, where the $\epsilon\text{Hf(t)}$ isotopic anomaly is transformed, is a potential prospective area for porphyry Mo-W(-Cu) deposits. This study shows that Hf isotope mapping can reveal the regional metallogenic rules and explore metallogenic prediction and metallogenic potential evaluation. Hf isotope mapping can be an expected new direction for studying regional metallogenic regularity, including, especially, studies of the detection and metallogenic background of deep crustal material.

Author Contributions: Conceptualisation, B.D., L.Y. and Z.Y.; methodology, B.D. and G.L.; software, L.W. and J.L.; validation, B.D.; formal analysis, B.D. and Q.C.; investigation, B.D., Z.Y., L.Y., Q.C., J.Z., K.S. and G.L.; writing—original draft preparation, B.D., Z.Y., K.S. and G.L.; writing—review and editing, B.D. and Z.Y.; visualisation, B.D. and Z.Y.; supervision, B.D. project administration, B.D. All authors have read and agreed to the published version of the manuscript.

Funding: This research is jointly supported by the National Natural Science Foundation of China (Numbers 41872080, 92162101), the most Special Fund from the State Key Laboratory of Geological Processes and Mineral Resources, China University of Geosciences (Number MSFGPMR201804).

Institutional Review Board Statement: Not applicable.

Informed Consent Statement: Not applicable.

Data Availability Statement: Not applicable.

Acknowledgments: The authors thank the team members at CUGB for their field support, data analysis, constructive discussions, and comments.

Conflicts of Interest: The authors declare no conflict of interest.

References

1. Lu, G.A. On effects of the geophysical prospecting method applied in volcanic sulphide search. *J. Cent. South Univ. Technol.* **1995**, *3*, 295–299.
2. Wang, Z.H.; Lu, Q.T.; Yan, J.Y. Review of geophysics for gold deposit. *Prog. Geophys.* **2016**, *31*, 805–813.
3. Xie, X.J.; Liu, D.W. Geochemical Mapping and Geochemical Exploration. *Geol. Rev.* **2006**, *52*, 721–732.
4. Li, H.; Zhang, G.Y.; Yu, B.; Li, D.L. Structural superimposed halos method for prospecting blind ore-body in the deep of ore-districts. *Earth Sci. Fron.* **2010**, *17*, 287.
5. Ma, J.W.; Ao, H.H.; Chen, S.D.; Zhang, T.Y. *Qinling-Gold Remote Sensing Geology*; Geological Publishing House: Beijing, China, 1997; pp. 1–200.
6. Xue, C.S.; Fu, X.L.; Wang, J.M. Fusion processing of remote sensing and geo-physical data and its application in geology—An example in Shangrao area. *Geol. Sci. and Technol. Inform.* **1997**, *(S1)*, 36–43.
7. Sabins, F.F. Remote sensing for mineral exploration. *Ore Geol. Rev.* **1999**, *1*, 157–183. [[CrossRef](#)]
8. Di Tommaso, I.; Rubinstein, N. Hydrothermal alteration mapping using ASTER data in the Infiernillo porphyry deposit, Argentina. *Ore Geol. Rev.* **2007**, *32*, 275–290. [[CrossRef](#)]
9. Cheng, T.W.; Chen, J.G.; Xu, M.Y. Application of mixed pixel decomposition in mineralization and alteration information extraction in vegetation-covered area: A case study of the Dahaoshan gold deposit in Jiangxi Province. *J. Geol.* **2017**, *41*, 492–498.
10. Xiong, S.Q. The role of aeromagnetic survey in the exploration of copper deposits in Sanjiang region, Southwest China. *Geophys. Explor.* **1998**, *1*, 43–48.
11. El-Sadek, M.A. Radiospectrometric and magnetic signatures of a gold mine in Egypt. *J. Appl. Geophys.* **2009**, *67*, 34–43. [[CrossRef](#)]
12. Wang, J.C.; Song, C.Y.; Wang, Z.L.; Zhou, L.L.; Zhang, Z.F.; Hu, Q.E. A comprehensive comparative study of geological characteristics as well as aeromagnetic and aeroradiometric features of the Bayan Obo REE–Nb–Fe deposits and their implications for prospecting work. *Geol. China* **2016**, *43*, 594–606.
13. Ballard, J.R.; Palin, J.M.; Campbell, I.H. Relative oxidation states of magmas inferred from Ce(IV)/Ce(III) in zircon: Application to porphyry copper deposits of northern Chile. *Contrib. Mineral. Petrol.* **2002**, *144*, 347–364. [[CrossRef](#)]

14. McCuaig, T.C.; Hronsky, J.M.A. The mineral system concept: The key to exploration targeting. *SEG Spec. Pub.* **2014**, *18*, 153–175. [[CrossRef](#)]
15. Lu, Y.J.; Loucks, R.R.; Fiorentini, M.L.; McCuaig, T.C.; Evans, N.J.; Yang, Z.M.; Hou, Z.Q.; Kirkland, C.L.; Parra-Avila, L.A.; Kobussen, A. Zircon compositions as a pathfinder for porphyry Cu ± Mo ± Au deposits. *SEG Spec. Pub.* **2016**, *19*, 329–347.
16. Hou, Z.Q.; Duan, L.F.; Lu, Y.J.; Zheng, Y.C.; Zhu, D.C.; Yang, Z.M.; Yang, Z.S.; Wang, B.D.; Pei, Y.R.; Zhao, Z.D.; et al. Lithospheric architecture of the Lhasa Terrane and its control on ore deposits in the Himalayan-Tibetan Orogen. *Econ. Geol.* **2015**, *110*, 1541–1575. [[CrossRef](#)]
17. Wang, C.M.; Leon, B.; Lu, Y.J.; Santosh, M.; Du, B.; McCuaig, T.C. Terrane boundary and spatio-temporal distribution of ore deposits in the Sanjiang Tethyan Orogen: Insights from zircon Hf-isotopic mapping. *Earth-Sci. Rev.* **2016**, *156*, 39–65. [[CrossRef](#)]
18. Du, B.; Wang, C.M.; He, X.Y.; Yang, L.F.; Chen, J.Y.; Shi, K.X.; Luo, Z.; Xia, J.S. Advances in research of bulk-rock Nd and zircon Hf isotopic mappings: Case study of the Sanjiang Tethyan Orogen. *Acta Petrol. Sin.* **2016**, *32*, 2555–2570.
19. Hou, Z.Q.; Wang, T. Isotopic mapping and deep material probing (I); imaging crustal architecture and its control on mineral systems. *Earth Sci. Front.* **2018**, *25*, 20–41.
20. Mole, D.R.; Fiorentini, M.L.; Thebaud, N.; Cassidy, K.F.; McCuaig, T.C.; Kirkland, C.L.; Romano, N.; Belousova, E.A.; Barnes, S.J.; Mill, J. Archean komatiite volcanism controlled by the evolution of early continents. *Proc. Natl. Acad. Sci. USA* **2014**, *111*, 10083–10088. [[CrossRef](#)]
21. Mole, D.R.; Fiorentini, M.L.; Cassidy, K.F.; Kirkland, C.L.; Romano, N.; Maas, R.; Belousova, E.A.; Barnes, S.J.; Mill, J. Crustal evolution, intra-cratonic architecture and the metallogeny of an Archaean Craton. *Geol. Soc. Lond. Spec. Pub.* **2015**, *393*, 23–80. [[CrossRef](#)]
22. Wang, C.M.; Deng, J.; Bagas, L.; Wang, Q. Zircon Hf-isotopic mapping for understanding crustal architecture and metallogenesis in the Eastern Qinling Orogen. *Gondwana Res.* **2017**, *50*, 293–310. [[CrossRef](#)]
23. Wang, C.M.; Bagas, L.; Deng, J.; Dong, M.M. Crustal architecture and its controls on mineralisation in the North China Craton. *Ore Geol. Rev.* **2018**, *98*, 109–125. [[CrossRef](#)]
24. Deng, J.; Wang, C.M.; Bagas, L.; Santosh, M.; Yao, E.Y. Crustal architecture and metallogenesis in the south-eastern North China Craton. *Earth-Sci. Rev.* **2018**, *182*, 251–272. [[CrossRef](#)]
25. Wang, T.; Jahn, B.M.; Kovach, V.P.; Tong, Y.; Hong, D.W.; Han, B.F. Nd-Sr isotopic mapping of the Chinese Altai and implications for continental growth in the Central Asian Orogenic Belt. *Lithos* **2009**, *110*, 359–372. [[CrossRef](#)]
26. Wang, T.; Hou, Z.Q. Isotopic mapping and deep material probing (I) revealing the compositional evolution of the lithosphere and crustal growth processes. *Earth Sci. Front.* **2018**, *25*, 1–19.
27. Zhang, L.X.; Wang, Q.; Zhu, D.C.; Jia, L.L.; Wu, X.Y.; Liu, S.A.; Hu, Z.C.; Zhao, T.P. Mapping the Lhasa Terrane through zircon Hf isotopes: Constraints on the nature of the crust and metallogenic potential. *Acta Petrol. Sin.* **2013**, *29*, 3681–3688.
28. Deng, J.; Wang, C.M.; Li, G.J. Style and process of the superimposed mineralization in the Sanjiang Tethys. *Acta Petrol. Sin.* **2012**, *28*, 1349–1361.
29. Deng, J.; Wang, Q.F.; Chen, F.C.; Li, G.J.; Yang, L.Q.; Wang, C.M.; Zhang, J.; Sun, X.; Su, Q.H.; He, W.Y.; et al. Further discussion on the Sanjiang Tethyan composite metallogenic system. *Earth Sci. Front.* **2020**, *27*, 106–136.
30. Deng, J.; Wang, Q.F.; Li, G.J.; Santosh, M. Cenozoic tectono-magmatic and metallogenic processes in the Sanjiang region, Southwestern China. *Earth Sci. Rev.* **2014**, *138*, 268–299. [[CrossRef](#)]
31. Deng, J.; Wang, Q.F.; Li, G.J.; Li, C.S.; Wang, C.M. Tethys evolution and spatial-temporal distribution of ore deposits in the Sanjiang region, Southwestern China. *Gondwana Res.* **2014**, *26*, 419–437. [[CrossRef](#)]
32. Deng, J.; Wang, Q.F.; Li, G.J. Tectonic evolution, superimposed orogeny, and composite metallogenic system in China. *Gondwana Res.* **2017**, *50*, 216–266. [[CrossRef](#)]
33. Li, G.J. Tethys Tectonic Evolution and Metallogenesis of Important Mineral Deposits in the Sanjiang Region, SW China. Ph.D. Thesis, China University of Geosciences, Beijing, China, 2014.
34. Deng, J.; Wang, C.M.; Li, G.J.; Zhou, D.Q. The theory of composite metallogenic system: Key of recovering metallogenic mystery in the SW Tethys. *Acta Petrol. Sin.* **2019**, *35*, 1303–1323.
35. Wang, X.X.; Wang, T.; Ke, C.H. Nd-Hf isotopic mapping of Late Mesozoic granitoids in the East Qinling orogen, central China: Constraint on the basements of terranes and distribution of Mo mineralization. *J. Asian Earth Sci.* **2015**, *103*, 169–183. [[CrossRef](#)]
36. Wang, C.M.; Deng, J.; Bagas, L.; He, X.Y.; Zhang, J. Origin and classification of the Late Triassic Huaishuping gold deposit in the eastern part of the Qinling-Dabie Orogen, China: Implications for gold metallogeny. *Miner. Depos.* **2021**, *56*, 725–742. [[CrossRef](#)]
37. Zhou, D.Q. The Deep Tectonic-Magmatic System and Mineralization of Tethys Composite Orogenic Belt in Sanjiang Region. Ph.D. Thesis, China University of Geosciences, Beijing, China, 2013.
38. Du, B. Magma Source, Formation Mechanism and Tectonic Significance of the Dalianhuashan and Zhuopan Plutons, Yunan Province. Master's Thesis, China University of Geosciences, Beijing, China, 2017.
39. Deng, J.; Wang, Q.F. Gold mineralization in China: Metallogenic provinces, deposit types and tectonic framework. *Gondwana Res.* **2016**, *36*, 219–274. [[CrossRef](#)]
40. Du, B. Lithospheric Material Structure of the Sanjiang Tethys Orogenic Belt and Its Constraints on Porphyry Metallogenesis. Ph.D. Thesis, China University of Geosciences, Beijing, China, 2020.

41. Wang, C.M.; Yang, L.F.; Bagas, L.; Noreen, E.; Chen, J.Y.; Du, B. Mineralization processes at the giant Jinding Zn-Pb deposit, Lanping Basin, Sanjiang Tethys Orogen: Evidence from in-situ trace element analysis of pyrite and marcasite. *Geol. J.* **2018**, *53*, 1279–1294. [[CrossRef](#)]
42. Wang, C.M.; Bagas, L.; Chen, J.Y.; Yang, L.F.; Zhang, D.; Du, B.; Shi, K.X. The genesis of the Liancheng Cu-Mo deposit in the Lanping Basin of SW China: Constraints from geology, fluid inclusions, and Cu-S-H-O isotopes. *Ore Geol. Rev.* **2018**, *92*, 113–128. [[CrossRef](#)]
43. Zhou, D.Q.; Deng, J.; Cao, B.B.; Fan, Z.G.; Huang, X.Z.; Hu, X.W. Tethyan Composite Orogeny Process and its Constraints on Metallogenesis in Sanjiang Region, SW China. *Acta Geol. Sin.* **2014**, *88*, 950–951. [[CrossRef](#)]
44. Li, W.C.; Yin, G.H.; Yu, H.J.; Lu, Y.X.; Liu, X.L. The porphyry metallogenesis of Geza volcanic magmatic arc in NW Yunnan. *Acta Petrol. Sin.* **2011**, *27*, 2541–2552.
45. Li, W.C.; Yu, H.J.; Yin, G.H. Porphyry metallogenic system of Geza arc in the Sanjiang region, southwestern China. *Acta Petrol. Sin.* **2013**, *29*, 1129–1144.
46. Hou, Z.Q.; Ma, H.; Khin, Z.; Zhang, Y.; Wang, M.; Wang, Z.; Pan, G.; Tang, R. The Himalayan Yulong porphyry copper belt: Product of large-scale strike-slip faulting in eastern Tibet. *Econ. Geol.* **2003**, *98*, 125–145.
47. Lin, B.; Wang, L.; Tang, J.; Lin, B.; Wang, L.Q.; Tang, J.X.; Song, Y.; Cao, H.W.; Baker, M.J.; Zhang, L.J.; et al. Geology, geochronology, geochemical characteristics and origin of Baomai porphyry Cu (Mo) deposit, Yulong Belt, Tibet. *Ore Geol. Rev.* **2018**, *92*, 186–204. [[CrossRef](#)]
48. He, W.Y.; Yang, L.Q.; Brugger, J.; McCuaig, T.C.; Lu, Y.J.; Bao, X.S.; Gao, X.Q.; Lu, Y.G.; Xing, Y.L. Hydrothermal evolution and ore genesis of the Beiya giant Au polymetallic deposit, western Yunnan, China: Evidence from fluid inclusions and H-O-S-Pb isotopes. *Ore Geol. Rev.* **2017**, *90*, 847–862. [[CrossRef](#)]
49. Deng, J.; Wang, Q.F.; Li, G.J.; Hou, Z.Q.; Jiang, C.Z.; Danyushevsky, L. Geology and genesis of the giant Beiya porphyry-skarn gold deposit, northwestern Yangtze Block, China. *Ore Geol. Rev.* **2015**, *70*, 457–485. [[CrossRef](#)]
50. Xu, L.L.; Bi, X.W.; Hu, R.Z.; Qi, Y.Q.; Tang, Y.Y.; Wang, X.S.; Zhu, J.J. Redox states and genesis of magmas associated with intra-continental porphyry Cu-Au mineralization within the Jinshajiang-Red River alkaline igneous belt, SW China. *Ore Geol. Rev.* **2016**, *73*, 330–345. [[CrossRef](#)]
51. Zhu, X.P. Geological Characteristics and Metallogenesis in Habo Porphyry Cu-Mo-Au Deposit, Yunnan, China. Ph.D. Thesis, China University of Geosciences, Beijing, China, 2010.
52. He, W.Y.; Mo, X.X.; He, Z.H.; White, N.C.; Chen, J.B.; Yang, K.H.; Wang, R.; Yu, X.H.; Dong, G.C.; Huang, X.F. The geology and mineralogy of the Beiya skarn gold deposit in Yunnan, southwest China. *Econ. Geol.* **2015**, *110*, 1625–1641. [[CrossRef](#)]
53. Li, W.C.; Xue, Y.X.; Lu, Y.X.; Xue, S.R.; Ren, Z.J.; Chen, J.P.; Chen, Y.Q.; Liu, H.F.; Wang, Y.J.; Yue, C.T.; et al. *Metallogenic Rules of Porphyry Copper Ore in CHINA and the Direction of Mineralization Search*; Geological Publishing House: Beijing, China, 2014; pp. 1–424.
54. Liu, X.L.; Li, W.C.; Zhang, N.; Lai, A.Q.; Li, Z.; Yang, F.C. Metallogenic system of the Yanshanian porphyry Mo polymetallic deposit in the Xiangcheng-Lijiang suture zone, western margin of Yangtze block, SW China. *Acta Petrol. Sin.* **2016**, *32*, 2281–2302.
55. Li, W.C.; Yu, H.J.; Gao, X.; Liu, X.L.; Wang, J.H. Review of Mesozoic multiple magmatism and porphyry Cu-Mo (W) mineralization in the Yidun Arc, eastern Tibet Plateau. *Ore Geol. Rev.* **2017**, *90*, 795–812. [[CrossRef](#)]
56. Yu, H.J. Composite Metallogenic System and Exploration Research of the Geza Porphyry Belt, SW China. Ph.D. Thesis, China University of Geosciences, Beijing, China, 2018.
57. Wang, C.M.; Deng, J.; Carranza, E.J.M.; Santosh, M. Tin metallogenesis associated with granitoids in the southwestern Sanjiang Tethyan Domain: Nature, deposit types, and tectonic setting. *Gondwana Res.* **2013**, *26*, 576–593. [[CrossRef](#)]
58. Davis, D.W.; Amelin, Y.; Nowell, G.M.; Nowell, R.R. Parrish Hf isotopes in zircon from the western Superior province, Canada: Implications for Archean crustal development and evolution of the depleted mantle reservoir. *Precambrian Res.* **2005**, *140*, 132–156. [[CrossRef](#)]
59. Pollock, J.C.; Sylvester, P.J.; Barr, S.M. Lu-Hf zircon and Sm-Nd whole-rock isotope constraints on the extent of juvenile arc crust in Avalonia: Examples from Newfoundland and Nova Scotia, Canada. *Can. J. Earth Sci.* **2015**, *52*, 161–181. [[CrossRef](#)]
60. Griffin, W.L.; Wang, X.; Jackson, S.E.; Pearson, N.J.; O'Reilly, S.Y.; Xu, X.; Zhou, X. Zircon chemistry and magma mixing, SE China: In situ analysis of Hf isotopes, Tonglu and Pingtan igneous complexes. *Lithos* **2002**, *61*, 237–269. [[CrossRef](#)]
61. Wu, F.Y.; Li, X.H.; Yang, J.H.; Zheng, Y.F. Discussions on the petrogenesis of granites. *Acta Petrol. Sin.* **2007**, *23*, 1217–1238.
62. Chen, F.K.; Li, X.H.; Wang, X.L.; Li, Q.L.; Siebel, W. Zircon age and Nd-Hf isotopic composition of the Yunnan Tethyan belt, southwestern China. *Int. J. Earth Sci.* **2007**, *96*, 1179–1194. [[CrossRef](#)]
63. Reid, A.; Wilson, C.J.L.; Shun, L.; Pearson, N.; Belousova, E. Mesozoic plutons of the Yidun Arc, SW China: U/Pb geochronology and Hf isotopic signature. *Ore Geol. Rev.* **2007**, *3*, 88–106. [[CrossRef](#)]
64. Zhao, Y.J. Mesozoic Granitoids in Eastern Songpan-Garze: Geochemistry, Petrogenesis and Tectonic Implications. Ph.D. Thesis, Chinese Academy of Sciences, Guangzhou, China, 2007.
65. Liu, S.; Hu, R.Z.; Gao, S.; Feng, C.X.; Huang, Z.L.; Lai, S.C.; Yuan, H.L.; Liu, X.M.; Coulson, I.M.; Feng, G.Y.; et al. U-Pb zircon, geochemical and Sr-Nd-Hf isotope constraints on the age and origin of early Paleozoic I-type granite from the Tengchong-Baoshan Block, Western Yunnan Province, SW China. *Int. J. Earth Sci.* **2009**, *36*, 168–182.

66. Zhu, D.C.; Mo, X.X.; Wang, L.Q.; Zhao, Z.D.; Niu, Y.L.; Yang, Y.H. Petrogenesis of highly fractionated I-type granites in the Chayu area of eastern Gangdese, Tibet: Constraints from zircon U-Pb geochronology, geochemistry and Sr-Nd-Hf isotopes. *Sci. China Ser. D-Earth Sci.* **2009**, *39*, 833–848.
67. Cai, H.M.; Zhang, H.F.; Xu, W.C. U-Pb zircon ages, geochemical and Sr-Nd-Hf isotopic compositions of granitoids in western Songpan-Garze fold belt: Petrogenesis and implication for tectonic evolution. *J. Earth Sci.* **2009**, *20*, 681–698. [[CrossRef](#)]
68. Cai, H.M. Petrogenesis of Indosinian Granitoids and Volcanic Rocks in Songpan-Garze Fold Belt: Constraints for Deep Geologic Processes. Ph.D. Thesis, China University of Geosciences, Wuhan, China, 2010.
69. Tran, M.D.; Liu, J.L.; Nguyen, Q.L.; Chen, Y.; Ji, M.; Tang, Y. Zircon U Pb ages and H f isotopic composition of the PuSam Cap high potassic alkaline rocks in northwestern Vietnam and regional tectonic implication. *Acta Petrol. Sin.* **2010**, *26*, 1902–1914.
70. Wang, Y.B.; Han, J.; Zeng, P.S.; Wang, D.H.; Hou, K.J.; Yin, G.H.; Li, W.C. U-Pb dating and Hf isotopic characteristics of zircons from granodiorite in Yangla copper deposit, Deqin County, Yunnan, Southwest China. *Acta Petrol. Sin.* **2010**, *26*, 1833–1844.
71. Dong, X.H.; Peng, T.P.; Fan, W.M.; Zhao, G.C.; Zhang, J.Y.; Liu, B.B.; Gao, J.F.; Peng, B.X.; Liang, X.R.; Zeng, W.; et al. Origin and tectonic implications of Early Cretaceous high- and low-Mg series rocks and mafic enclaves in the Bomi-Chayu Fold Belt, SE Tibet. *Lithos* **2019**, *334*, 102–116. [[CrossRef](#)]
72. Wang, X.S.; Hu, R.Z.; Bi, X.W.; Leng, C.B.; Pan, L.C. Petrogenesis of Late Cretaceous I-type granites in the southern Yidun Terrane: New constraints on the Late Mesozoic tectonic evolution of the eastern Tibetan Plateau. *Lithos* **2014**, *208*, 202–219. [[CrossRef](#)]
73. Wang, X.S.; Bi, X.W.; Leng, C.B.; Zhong, H.; Tang, H.F.; Chen, Y.W.; Yin, G.H.; Huang, D.Z.; Zhou, M.F. Geochronology and geochemistry of Late Cretaceous igneous intrusions and Mo-Cu-(W) mineralization in the southern Yidun Arc, SW China: Implications for metallogenesis and geodynamic setting. *Ore Geol. Rev.* **2014**, *61*, 73–95. [[CrossRef](#)]
74. Qi, X.X.; Zhu, L.H.; Hu, Z.C.; Li, Z.Q. Zircon SHRIMP U-Pb dating and Lu-Hf isotopic composition for Early Cretaceous plutonic rocks in Tengchong block, southeastern Tibet, and its tectonic implications. *Acta Petrol. Sin.* **2011**, *27*, 3409–3421.
75. Zhu, J. Geological, Geochemical Characteristics and Genesis of the Yangla Copper Deposit, Deqin county, Yunnan. Ph.D. Thesis, Kunming University of Science and Technology, Kunming, China, 2011.
76. Zhu, J.J.; Hu, Z.; Bi, X.W.; Zhong, H.; Chen, H. Zircon U-Pb ages, Hf-O isotopes and whole-rock Sr-Nd-Pb isotopic geochemistry of granitoids in the Jinshajiang suture zone, SW China: Constraints on petrogenesis and tectonic evolution of the Paleo-Tethys Ocean. *Lithos* **2011**, *126*, 248–264. [[CrossRef](#)]
77. Dong, M.L.; Dong, G.C.; Mo, X.X.; Zhu, D.C.; Nie, F.; Xie, X.F.; Wang, X.; Hu, Z.C. Geochronology and geochemistry of the Early Palaeozoic granitoids in Baoshan block, western Yunnan and their implications. *Acta Petrol. Sin.* **2012**, *28*, 1453–1464.
78. Dong, M.L.; Dong, G.C.; Mo, X.X.; Zhu, D.C.; Nie, F.; Yu, J.C.; Wang, P.; Luo, W. The Mesozoic-Cenozoic magmatism in Baoshan Block, western Yunnan and its tectonic significance. *Acta Petrol. Sin.* **2013**, *29*, 3901–3913.
79. Dong, M.L.; Dong, G.C.; Mo, X.X.; Santosh, M.; Zhu, D.C.; Yu, J.C.; Nie, F.; Hu, Z.C. Geochemistry, zircon U-Pb geochronology and Hf isotopes of granites in the Baoshan Block, Western Yunnan: Implications for Early Paleozoic evolution along the Gondwana. *Lithos* **2013**, *179*, 36–47. [[CrossRef](#)]
80. Dong, G.C.; Mo, X.X.; Zhao, Z.D.; Zhu, D.C.; Goodman, R.C.; Kong, H.L.; Wang, S. Zircon U-Pb dating and the petrological and geochemical constraints on Lincang granite in western Yunnan, China: Implications for the closure of the Paleo-Tethys Ocean. *J. Asian Earth Sci.* **2013**, *62*, 282–294. [[CrossRef](#)]
81. Guo, L. The Tectono-Magma Events in the Western Margin of the Eastern Himalayan Syntaxis and Their Geodynamic Implications. Ph.D. Thesis, China University of Geosciences, Wuhan, China, 2012.
82. Leng, C.B.; Zhang, X.C.; Hu, R.Z.; Wang, S.X.; Zhong, H.; Wang, W.Q.; Bi, X.W. Zircon U-Pb and molybdenite Re-Os geochronology and Sr-Nd-Pb-Hf isotopic constraints on the genesis of the Xuejiping porphyry copper deposit in Zhongdian, Northwest Yunnan, China. *J. Asian Earth Sci.* **2012**, *60*, 31–48. [[CrossRef](#)]
83. Li, Z.H.; Lin, S.L.; Cong, F.; Zou, G.F.; Xie, T. Indosinian orogenesis of the Tengchong-Lianghe block, Western Yunnan: Evidence from zircon U-Pb dating and petrogenesis of granitoids. *Acta Petrol. Mineral.* **2010**, *29*, 298–312.
84. Li, Z.H.; Lin, S.L.; Cong, F.; Zou, G.F.; Xie, T. U-Pb dating and Hf isotopic compositions of quartz diorite and monzonitic granite from the Tengchong-Lianghe block, western Yunnan, and its geological implications. *Acta Geol. Sin.* **2012**, *86*, 1047–1061.
85. Jiang, B.; Gong, Q.J.; Zhang, J.; Ma, N. Late Cretaceous aluminum A-type granites and its geological significance of Dasongpo Sn deposit, Tengchong, West Yunnan. *Acta Petrol. Sin.* **2012**, *28*, 1477–1492.
86. Kong, H.L.; Dong, G.C.; Mo, X.X.; Zhao, Z.D.; Zhu, D.C.; Wang, S.; Li, R.; Wang, Q.L. Petrogenesis of the Lincang granites in Sanjiang area of western Yunnan Province: Constraints from geochemistry, zircon U-Pb geochronology and Hf isotope. *Acta Geol. Sin.* **2012**, *28*, 1438–1452.
87. Xu, Y.G.; Yang, Q.J.; Lan, J.B.; Luo, Z.Y.; Huang, X.L.; Shi, Y.R.; Xie, L.W. Temporal-spatial distribution and tectonic implications of the batholiths in the Gaoligong-Tengliang-Yingjiang area, western Yunnan: Constraints from zircon U-Pb ages and Hf isotopes. *Int. J. Earth Sci.* **2012**, *53*, 151–175. [[CrossRef](#)]
88. Zi, J.W.; Cawood, P.A.; Fan, W.M.; Tohver, E.; Wang, Y.J.; McCuaig, T.C. Generation of Early Indosinian enriched mantle-derived granitoid pluton in the Sanjiang Orogen (SW China) in response to closure of the Paleo-Tethys. *Lithos* **2012**, *140*, 166–182. [[CrossRef](#)]
89. Zi, J.W.; Cawood, P.A.; Fan, W.M.; Wang, Y.J.; Tohver, E.; McCuaig, T.C.; Peng, T.P. Triassic collision in the Paleo-Tethys Ocean constrained by volcanic activity in SW China. *Lithos* **2012**, *144*, 145–160. [[CrossRef](#)]

90. He, D.F.; Zhu, W.G.; Zhong, H.; Ren, T.; Bai, Z.J.; Fan, H.P. Zircon U-Pb geochronology and elemental and Sr-Nd-Hf isotopic geochemistry of the Daocheng granitic pluton from the Yidun Arc, SW China. *J. Asian Earth Sci.* **2013**, *67*, 1–17. [CrossRef]
91. Li, H.Q.; Xu, Z.Q.; Wang, R.R.; Dong, H.W.; Sun, Z.B.; Huang, X.M. Petrogenesis and tectonic significance of the Late Jurassic granite discovered in the Bomi-Chayu region, eastern Tibet. *Acta Petrol. Sin.* **2013**, *29*, 2024–2032.
92. Li, W.K.; Xie, J.C.; Dong, G.C.; Mo, X.X.; Zhao, Z.D.; Wang, T.C. The geochronology and geochemistry of Bomi granitoids in eastern Tibet and its significance. *Acta Petrol. Sin.* **2013**, *29*, 3745–3754.
93. Lin, J.Z. Geological and Geochemical Characteristics of Lailishan Granites in Tengchong Tin Belt, Western Yunnan, and Their Relation to Mineralization. Master’s Thesis, China University of Geosciences, Wuhan, China, 2013.
94. Lu, Y.J.; Kerrich, R.; Kemp, A.I.S.; McCuaig, T.C.; Hou, Z.Q.; Hart, C.J.R.; Li, Z.X.; Cawood, P.A.; Bagas, L.; Yang, Z.M.; et al. Intracontinental Eocene-Oligocene porphyry Cu mineral systems of Yunnan, western Yangtze craton, China: Compositional characteristics, sources, and implications for continental collision metallogeny. *Econ. Geol.* **2013**, *108*, 1541–1576. [CrossRef]
95. Lu, Y.J.; Kerrich, R.; McCuaig, T.C.; Li, Z.X.; Hart, C.J.R.; Cawood, P.A.; Hou, Z.Q.; Bagas, L.; Cliff, J.; Belousova, E.A.; et al. Geochemical, Sr-Nd-Pb, and zircon Hf-O isotopic compositions of Eocene-Oligocene shoshonitic and potassic Adakite-like felsic intrusions in Western Yunnan, SW China: Petrogenesis and tectonic implications. *J. Petrol.* **2013**, *54*, 1309–1348. [CrossRef]
96. Li, G.J.; Wang, Q.F.; Yu, L.; Hu, Z.C.; Ma, N.; Huang, Y.H. Closure time of the Ailaoshan Paleo-Tethys Ocean: Constraints from the zircon U-Pb dating and geochemistry of the Late Permian granitoids. *Acta Petrol. Sin.* **2013**, *29*, 3883–3900.
97. Liu, H.C.; Wang, Y.J.; Cai, Y.F.; Ma, L.Y.; Xing, X.W.; Fan, W.M. Zircon U-Pb geochronology and Hf isotopic composition of the Xin’anzhai granite along the Ailaoshan tectonic zone in west Yunnan Province. *Geotecton. Metallog.* **2013**, *37*, 87–98.
98. Liu, X.L.; Li, W.C. The Indo Chinese epoch magmatism in Gega Arc of Yunnan: Evidences from zircon U-Pb dating and Hf isotopic composition. *Earth Sci. Front.* **2013**, *20*, 57–74.
99. Peng, T.P.; Wilde, S.A.; Wang, Y.J.; Fan, W.M.; Peng, B.X. Mid-Triassic felsic igneous rocks from the southern Lancangjiang Zone, SW China: Petrogenesis and implications for the evolution of Paleo-Tethys. *Lithos* **2013**, *168*, 15–32. [CrossRef]
100. Peng, T.P.; Zhao, G.C.; Fan, W.M.; Peng, B.X.; Mao, Y.S. Zircon geochronology and Hf isotopes of Mesozoic intrusive rocks from the Yidun terrane, Eastern Tibetan Plateau: Petrogenesis and their bearings with Cu mineralization. *Int. J. Earth Sci.* **2014**, *80*, 18–33. [CrossRef]
101. Xie, J.C.; Li, W.K.; Dong, G.C.; Mo, X.X.; Zhao, Z.D.; Yu, J.C.; Wang, T.C. Petrology, geochemistry and tectonic significance of the granites from Basu area, Tibet. *Acta Petrol. Sin.* **2013**, *29*, 3779–3791.
102. Bu, X.F. Geochemistry, Geochronology and Space-Time Evolvement of Granites in Nujiang Area of Northwestern Yunnan. Master’s Thesis, China University of Geosciences, Beijing, China, 2014.
103. Gao, Y.J.; Lin, S.L.; Cong, F.; Zou, G.F.; Xie, T.; Tang, F.W.; Li, Z.H.; Liang, T. Zircon U-Pb geochronology, zircon Hf isotope and bulk geochemistry of Paeogene granite in the Tengchong-Lianghe area, western Yunnan. *Acta Geol. Sin.* **2014**, *88*, 63–71.
104. Liu, H.C.; Wang, Y.J.; Fan, W.M.; Zi, J.W.; Cai, Y.F.; Yang, G.L. Petrogenesis and tectonic implications of Late-Triassic high ϵ Nd (t)- ϵ Hf (t) granites in the Ailaoshan tectonic zone (SW China). *Sci. China Earth Sci.* **2014**, *57*, 2181–2194. [CrossRef]
105. Li, Y.J.; Wei, J.H.; Chen, H.Y.; Li, H.; Chen, C.; Hou, B.J. Petrogenesis of the Xiasai Early Cretaceous A-type granite from the Yidun island arc belt, SW China: Constraints from Zircon U-Pb Age, Geochemistry and Hf Isotope. *Geotecton. Metallog.* **2014**, *38*, 939–953.
106. Ma, N. Magmatism and Mineralization in the Tengchong Tin-Polymetallic Metallogenic Belt. Ph.D. Thesis, China University of Geosciences, Beijing, China, 2014.
107. Wang, B.D.; Wang, L.; Chen, J.; Yin, F.G.; Wang, D.B.; Zhang, W.P.; Chen, L.K.; Liu, H. Triassic three-stage collision in the Paleo-Tethys: Constraints from magmatism in the Jiangda-Deqen-Weixi continental margin arc, SW China. *Gondwana Res.* **2014**, *26*, 475–491. [CrossRef]
108. Wu, T.; Xiao, L.; Gao, R.; Yang, H.J.; Yang, G. Petrogenesis and tectonic setting of the Que’ershan composite granitic pluton, Eastern Tibetan Plateau: Constraints from geochronology, geochemistry and Hf isotope data. *Sci. China Earth Sci.* **2014**, *44*, 1791–1806.
109. Yu, L.; Li, G.J.; Wang, Q.F.; Liu, X.F. Petrogenesis and tectonic significance of the Late Cretaceous magmatism in the northern part of the Baoshan block: Constraints from bulk geochemistry, zircon U-Pb geochronology and Hf isotopic compositions. *Acta Petrol. Sin.* **2014**, *30*, 2709–2724.
110. Yu, L.; Wang, Q.F.; Li, G.J.; Gao, L. Geochemistry, zircon U-Pb geochronology of granitic pegmatites from Caojian area in the north of Baoshan block, and their geological significance. *Acta Petrol. Sin.* **2015**, *31*, 3281–3296.
111. Yang, Z.; Hou, Z.; Xu, J.; Bian, X.; Yang, Z.; Tian, S.; Liu, Y.; Wang, Z. Geology and origin of the post-collisional Narigongma porphyry Cu-Mo deposit, southern Qinghai, Tibet. *Gondwana Res.* **2014**, *26*, 536–556. [CrossRef]
112. Zhang, J.; Deng, J.; Chen, H.Y.; Yang, L.Q.; Cooke, D.; Danyushevsky, L.; Gong, Q.J. LA-ICP-MS trace element analysis of pyrite from the Chang’an gold deposit, Sanjiang region, China: Implication for ore-forming process. *Gondwana Res.* **2014**, *26*, 557–575. [CrossRef]
113. Zhao, S.W.; Lai, S.C.; Qin, J.F.; Zhu, R.Z. Zircon U-Pb ages, geochemistry, and Sr-Nd-Pb-Hf isotopic compositions of the Pinghe pluton, Southwest China: Implications for the evolution of the early Palaeozoic Proto-Tethys in Southeast Asia. *Int. Geol. Rev.* **2014**, *56*, 885–904. [CrossRef]
114. Wu, T.; Xiao, L.; Wilde, S.A.; Ma, C.Q.; Zhou, J.X. A mixed source for the Late Triassic Garzê-Daocheng granitic belt and its implications for the tectonic evolution of the Yidun arc belt, eastern Tibetan Plateau. *Lithos* **2017**, *288*, 214–230. [CrossRef]

115. Cao, H.W. Research on Mesozoic-Cenozoic Magmatic Evolution and Its Relation with Metallogeny in Tengchong-Lianghe Tin Ore Belt, Western Yunnan. Ph.D. Thesis, China University of Geosciences, Beijing, China, 2015.
116. Cao, H.W.; Zhang, S.T.; Lin, J.Z.; Zheng, L.; Wu, J.D.; Li, D. Geology, geochemistry and geochronology of the Jiaojiguanliangzi Fe-polymetallic deposit, Tengchong County, Western Yunnan (China): Regional tectonic implications. *J. Asian Earth Sci.* **2014**, *81*, 142–152. [[CrossRef](#)]
117. Cai, Y.F.; Wang, Y.J.; Cawood, P.A.; Zhang, Y.Z.; Zhang, A.M. Neoproterozoic crustal growth of the Southern Yangtze Block: Geochemical and zircon U-Pb geochronological and Lu-Hf isotopic evidence of Neoproterozoic diorite from the Ailaoshan zone. *Precambrian Res.* **2015**, *266*, 137–149. [[CrossRef](#)]
118. Deng, J.; Wang, C.M.; Zi, J.W.; Xia, R.; Li, Q. Constraining subduction-collision processes of the Paleo-Tethys along the Changning-Menglian Suture: New zircon U-Pb ages and Sr-Nd-Pb-Hf-O isotopes of the Lincang Batholith. *Gondwana Res.* **2018**, *62*, 75–92. [[CrossRef](#)]
119. Deng, J.; Wang, Q.F.; Li, G.J.; Zhao, Y. Structural control and genesis of the Oligocene Zhenyuan orogenic gold deposit, SW China. *Ore Geol. Rev.* **2015**, *65*, 42–54. [[CrossRef](#)]
120. Jiang, L.L.; Xue, C.D.; Hou, Z.Q.; Xiang, K. Petrogenesis of the Bengge syenites, Northeastern Yunnan: Geochemistry, geochronology and Hf isotopes evidence. *Acta Petrol. Sin.* **2015**, *11*, 3234–3246.
121. Liu, H.C.; Wang, Y.J.; Cawood, P.A.; Fan, W.M.; Cai, Y.F.; Xing, X.W. Record of Tethyan ocean closure and Indosinian collision along the Ailaoshan suture zone (SW China). *Gondwana Res.* **2015**, *27*, 1292–1306. [[CrossRef](#)]
122. Cao, K.; Xu, J.F.; Chen, J.L.; Huang, X.X.; Ren, J.B.; Zhao, X.D.; Liu, Z.X. Double-layer structure of the crust beneath the Zhongdian arc, SW China: U-Pb geochronology and Hf isotope evidence. *J. Asian Earth Sci.* **2016**, *115*, 455–467. [[CrossRef](#)]
123. Dong, M.L. Study of Magmatism in Tengchong-Baoshan Block, Western Yunnan and Its Tectonic Implications. Ph.D. Thesis, China University of Geosciences, Beijing, China, 2016.
124. Chen, X.L.; Huang, W.T.; Zou, Y.Q.; Liang, H.Y.; Zhang, J.; Zhang, Y.Q. Zircon U-Pb geochronology and geochemistry of ore-bearing porphyries in the southern Yulong porphyry copper belt and factors resulting in the differences in scale of mineralization between the southern and northern Yulong porphyry copper belt. *Acta Petrol. Sin.* **2016**, *32*, 2522–2534.
125. Ding, H.X.; Hou, Q.Q.; Zhang, Z.M. Petrogenesis and tectonic significance of the Eocene adakite-like rocks in western Yunnan, southeastern Tibetan Plateau. *Lithos* **2016**, *245*, 161–173. [[CrossRef](#)]
126. Li, G.J.; Wang, Q.F.; Yu, L.; Huang, Y.H.; Gao, L.; Li, Y. Petrogenesis of middle Ordovician peraluminous granites in the Baoshan block: Implications for the early Paleozoic tectonic evolution along East Gondwana. *Lithos* **2016**, *245*, 76–92. [[CrossRef](#)]
127. Xie, J.C.; Zhu, D.C.; Dong, G.; Dong, G.C.; Zhao, Z.D.; Wang, Q.; Mo, X.X. Linking the Tengchong Terrane in SW Yunnan with the Lhasa Terrane in southern Tibet through magmatic correlation. *Gondwana Res.* **2016**, *39*, 217–229. [[CrossRef](#)]
128. Wang, N.; Wu, C.L.; Qin, H.P.; Lei, M.; Guo, W.F.; Zhang, X.; Chen, H.J. Zircon UHPb Geochronology and Hf Isotopic Characteristics of the Daocheng Granite and Haizishan Granite in the Yidun Arc, Western Sichuan, and Their Geological Significance. *Acta Geol. Sin.* **2016**, *90*, 3227–3245.
129. Yu, L. Genesis and Tectonic Significance of the Mesozoic Granitoids in the Tengchong-Baoshan Block, Sanjiang Area. Ph.D. Thesis, China University of Geosciences, Beijing, China, 2016.
130. Zhao, S.W.; Lai, S.C.; Qin, J.F.; Zhu, R.Z. Petrogenesis of Eocene granitoids and microgranular enclaves in the western Tengchong Block: Constraints on eastward subduction of the Neo-Tethys. *Lithos* **2016**, *264*, 96–107. [[CrossRef](#)]
131. Zhao, S.W.; Lai, S.C.; Qin, J.F.; Zhu, R.Z. Tectono-magmatic evolution of the Gaoligong belt, southeastern margin of the Tibetan plateau: Constraints from granitic gneisses and granitoid intrusions. *Gondwana Res.* **2016**, *35*, 238–256. [[CrossRef](#)]
132. Zhao, S.W.; Lai, S.C.; Qin, J.F.; Zhu, R.Z.; Wang, J.B. Geochemical and geochronological characteristics of Late Cretaceous to Early Paleocene granitoids in the Tengchong Block, Southwestern China: Implications for crustal anatexis and thickness variations along the eastern Neo-Tethys subduction zone. *Tectonophysics* **2017**, *694*, 87–100. [[CrossRef](#)]
133. Chen, J.L.; Xu, J.F.; Ren, J.B.; Huang, X.X. Late Triassic E-MORB-like basalts associated with porphyry Cu-deposits in the southern Yidun continental arc, eastern Tibet: Evidence of slab-tear during subduction? *Ore Geol. Rev.* **2017**, *90*, 1054–1062. [[CrossRef](#)]
134. Han, M.Z. Alkali-Rich Porphyry Petrology and Geochemistry in Jianchuan in Yunnan Province. Master's Thesis, China University of Geosciences, Beijing, China, 2017.
135. Wu, J.; Liang, H.Y.; Mo, J.H.; Zhang, Y.Q.; Hu, G.Q. Petrochemistry and zircon LA-ICP-MS U-Pb age of the Mangzong porphyry associated with Cu-Mo mineralization in the Yulong ore belt. *Geotecton. Metallog.* **2011**, *35*, 300–306.
136. Wu, T. Early Mesozoic Magmatism and Tectonic Evolution of Yidun Arc Belt, Eastern Tibet Plateau. Ph.D. Thesis, China University of Geosciences, Wuhan, China, 2015.
137. Zhou, S.X.; Zhu, D.C.; Zhang, L.L.; Xie, J.C.; Wang, Q. Zircon U-Pb age and petrogenesis of the Permian highly fractionated granites in Tongpu, eastern Tibet. *Acta Petrol. Sin.* **2017**, *33*, 2509–2522.
138. Si, M. Isotopic Characteristics and Sources of Zirconium Heteriasis in Mesozoic Magmatic Rocks of Yidun Island. Master's Thesis, Chengdu University of Technology, Chengdu, China, 2017.
139. Zhao, Y.X. The Geochronology, Geochemistry of the Jiudingshan and Baofengsi Porphyry in Dali Yunnan. Master's Thesis, China University of Geosciences, Beijing, China, 2017.
140. Fan, Y.; Zhang, Y.H.; Zhang, S.T.; Cao, H.W.; Zou, H.; Dong, J.H. Early Cretaceous I-type granites in the Tengchong terrane: New constraints on the late Mesozoic tectonic evolution of southwestern China. *Geosci. Front.* **2018**, *9*, 459–470.

141. Zhou, S.X. Petrogenesis Implications of the Late Triassic Ludian Granite Batholith in Northwestern Yunnan. Master's Thesis, China University of Geosciences, Beijing, China, 2018.
142. He, W.Y.; Xie, S.X.; Liu, X.D.; Gao, X.; Xing, Y.L. Geochronology and geochemistry of the Donglufang porphyry-skarn Mo-Cu deposit in the southern Yidun Terrane and their geological significances. *Geosci. Front.* **2018**, *9*, 1433–1450. [[CrossRef](#)]
143. He, W.Y.; Yang, L.Q.; Lu, Y.J.; Jeon, H.; Xie, S.X.; Gao, X. Zircon U-Pb dating, geochemistry and Sr-Nd-Hf-O isotopes for the Baimaxueshan granodiorites and mafic microgranular enclaves in the Sanjiang Orogen: Evidence for westward subduction of Paleo-Tethys. *Gondwana Res.* **2018**, *62*, 112–126. [[CrossRef](#)]
144. Zhou, J.; Li, S.Z.; Wang, G.H.; Santosh, M.; Zhang, L.; Yu, S.Y.; Liu, Y.M.; Li, X.Y. Petrogenesis of Eocene mineralized porphyry in Bijiashan, eastern margin of Tibet Plateau: Constraints from geochronology, geochemistry and Hf isotopes. *Lithos* **2018**, *316*, 1–18.
145. Zhang, J.Y.; Peng, T.P.; Fan, W.M.; Zhao, G.C.; Dong, X.H.; Gao, J.F.; Peng, B.X.; Wei, C.; Xia, X.P.; Chen, L.L.; et al. Petrogenesis of the Early Cretaceous granitoids and its mafic enclaves in the Northern Tengchong Terrane, southern margin of the Tibetan Plateau and its tectonic implications. *Lithos* **2018**, *318*, 283–298. [[CrossRef](#)]
146. Zhang, Q.W.; Wang, Q.F.; Li, G.J.; Cui, X.L. Fractionation process of high-silica magmas through the lens of zircon crystallization: A case study from the Tengchong Block, SW China. *Chem. Geol.* **2018**, *496*, 34–42. [[CrossRef](#)]
147. Xia, B.; Lu, Y.; Yuan, Y.J.; Chen, W.Y.; Zhang, X.; Xu, C.; Yu, S.R.; Wan, Z.F. Mixing of Enriched Lithospheric Mantle-Derived and Crustal Magmas: Evidence from the Habo Cenozoic Porphyry in Western Yunnan. *Acta Geol. Sin.* **2018**, *92*, 1753–1768. [[CrossRef](#)]
148. Tong, X.; Zhao, Z.D.; Niu, Y.L.; Zhang, S.Q.; Cousens, B.; Liu, D.; Zhang, Y.; Han, M.Z.; Zhao, Y.X.; Lei, H.S. Petrogenesis and tectonic implications of the Eocene-Oligocene potassio felsic suites in western Yunnan, eastern Tibetan Plateau: Evidence from petrology, zircon chronology, elemental and Sr-Nd-Pb-Hf isotopic geochemistry. *Lithos* **2019**, *340*, 287–315. [[CrossRef](#)]
149. Zhou, S.M. Petrogenesis of the Late Triassic-Early Eocene Granitoids in the Tengchong Block. Ph.D. Thesis, China University of Geosciences, Beijing, China, 2019.
150. Zhou, Y.; Xu, B.; Hou, Z.Q.; Wang, R.; Zheng, Y.C.; He, W.Y. Petrogenesis of Cenozoic high-Sr/Y shoshonites and associated mafic microgranular enclaves in an intracontinental setting: Implications for porphyry Cu-Au mineralization in western Yunnan, China. *Lithos* **2019**, *324*, 39–54. [[CrossRef](#)]
151. Wu, J.K.; Zhao, Z.D.; Yang, Y.Y.; Lei, H.S.; Miao, Z.; Liu, D.; Zhu, D.C.; Yu, X.H. Petrogenesis and geological implications of the alkali-rich porphyry in southern Ailaoshan-Red River shear zone. *Acta Petrol. Sin.* **2019**, *35*, 485–504.
152. Du, B.; Wang, C.M.; Yang, L.F.; Shi, K.X.; Chen, Q.; Zhu, J.X. Petrogenesis of the Cenozoic Lianhuashan pluton (SW China): Constrained by zircon U-Pb geochronology, Lu-Hf isotope and geochemistry. *Geol. J.* **2020**, *5*, 3377–3400. [[CrossRef](#)]
153. Huang, M.L.; Bi, X.W.; Hu, R.Z.; Gao, J.F.; Xu, L.L.; Zhu, J.J.; Shang, L.B. Geochemistry, in-situ Sr-Nd-Hf-O isotopes, and mineralogical constraints on origin and magmatic-hydrothermal evolution of the Yulong porphyry Cu-Mo deposit, Eastern Tibet. *Gondwana Res.* **2019**, *76*, 98–114. [[CrossRef](#)]
154. Cao, D.H.; Wang, A.J.; Huang, Y.F.; Zhang, W.; Hou, K.J.; Li, R.P.; Li, Y.K. SHRIMP geochronology and Hf isotope composition of zircons from Xuejiping Porphyry copper deposit, Yunnan Province. *Acta Geol. Sin.* **2009**, *83*, 1430–1435.
155. Hennig, D.; Lehmann, B.; Frei, D.; Belyatsky, B.; Zhao, X.F.; Cabral, A.R.; Zeng, P.S.; Zhou, M.F.; Schmidt, K. Early Permian seafloor to continental arc magmatism in the eastern Paleo-Tethys: U-Pb age and Nd-Sr isotope data from the southern Lancangjiang Zone, Yunnan, China. *Lithos* **2009**, *113*, 408–422. [[CrossRef](#)]
156. Yang, L.Q.; Deng, J.; Dilek, Y.; Meng, J.Y.; Gao, X.; Santosh, M.; Wang, D.; Yan, H. Melt source and evolution of I-type granitoids in the SE Tibetan Plateau: Late Cretaceous magmatism and mineralization driven by collision-induced transtensional tectonics. *Gondwana Res.* **2016**, *245*, 258–273. [[CrossRef](#)]
157. Yang, L.Q.; Deng, J.; Gao, X.; He, W.Y.; Meng, J.Y.; Santosh, M.; Yu, H.J.; Yang, Z.; Wang, D. Timing of formation and origin of the Tongchanggou porphyry-skarn deposit: Implications for Late Cretaceous Mo-Cu metallogenesis in the southern Yidun Terrane, SE Tibetan Plateau. *Ore Geol. Rev.* **2017**, *81*, 1015–1032. [[CrossRef](#)]
158. Ren, J.B.; Xu, J.F.; Chen, J.L. Zircon geochronology and geological implications of ore-bearing bearing porphyries from Zhongdian arc. *Acta Petrol. Sin.* **2011**, *27*, 2591–2599.
159. Ren, J.B.; Xu, J.F.; Chen, J.L.; Zhang, S.Q.; Liang, H.Y. Geochemistry and petrogenesis of Pulang porphyries in Sanjiang region. *Acta Petrol. Mineral.* **2011**, *4*, 581–592.
160. Wang, C.M.; Deng, J.; Lu, Y.J.; Bagas, L.; Kemp, A.I.S.; McCuaig, T.C. Age, nature, and origin of Ordovician Zhibenshan granite from the Baoshan terrane in the Sanjiang region and its significance for understanding Proto-Tethys evolution. *Int. Geol. Rev.* **2015**, *57*, 1922–1939. [[CrossRef](#)]
161. Wang, C.M.; Deng, J.; Santosh, M.; McCuaig, T.C.; Lu, Y.J.; Carranza, E.J.M.; Wang, Q.F. Age and origin of the Bulangshan and Mengsong granitoids and their significance for post-collisional tectonics in the Changning-Menglian Paleo-Tethys Orogen. *J. Asian Earth Sci.* **2015**, *113*, 656–676. [[CrossRef](#)]
162. Chen, Q.; Wang, C.M.; Du, B.; Shi, K.X.; Yang, L.F.; Zhu, J.X.; Duan, H.Y. Petrogenesis of the Late Triassic Biluoqueshan granitic pluton, SW China: Implications for the tectonic evolution of the Paleo-Tethys Sanjiang Orogen. *J. Asian Earth Sci.* **2021**, *211*, 1367–9120. [[CrossRef](#)]
163. Mole, D.R.; Fiorentini, M.L.; Thebaud, N.; McCuaig, T.C.; Cassidy, K.F.; Kirkland, C.L.; Wingate, M.T.D.; Romano, S.S.; Doublier, M.P.; Belousova, E.A. Spatio-temporal constraints on lithospheric development in the southwest-central Yilgarn Craton, Western Australia. *Aust. J. Earth Sci.* **2012**, *59*, 625–656. [[CrossRef](#)]

164. Soderlund, U.; Patchett, P.J.; Vervoort, J.D.; Isachsen, C.E. The ^{176}Lu decay constant determined by Lu–Hf and U–Pb isotope systematics of Precambrian mafic intrusions. *Earth Planet. Sci. Lett.* **2004**, *219*, 311–324. [[CrossRef](#)]
165. Bouvier, A.; Vervoort, J.D.; Patchett, P.J. The Lu–Hf and Sm–Nd isotopic composition of CHUR: Constraints from unequilibrated chondrites and implications for the bulk composition of terrestrial planets. *Earth Planet. Sci. Lett.* **2008**, *273*, 48–57. [[CrossRef](#)]
166. Griffin, W.L.; Pearson, N.J.; Belousova, E.; Jackson, S.E.; van Achterbergh, E.; O'Reilly, S.Y.; Shee, S.R. The Hf isotope composition of cratonic mantle: LA-MC-ICPMS analysis of zircon megacrysts in kimberlites. *Geochim. Cosmochim. Acta* **2000**, *64*, 133–147. [[CrossRef](#)]
167. Zhang, S.M.; Xiao, Y.F.; Gong, T.T.; He, J.L.; Wang, Q.; Zhang, L.; Sun, J.D. Optimal Selection Assessment on Geochemical Anomalies at Gegongnong, Hengxinguo, Mamupu in the Yulong Metallogenic Zone, Tibet. *Bull. Mineral. Petrol. Geochem.* **2012**, *4*, 354–360.
168. Tang, R.L.; Luo, H.S. *The Geology of Yulong Porphyry Copper (Molybdenum) Ore Belt, Xizang (Tibet)*; Geological Publishing House: Beijing, China, 1995; 320p.
169. Hou, Z.Q.; Zaw, K.; Pan, G.T.; Xu, Q.; Hu, Y.; Li, X. Sanjiang Tethyan metallogenesis in S.W. China: Tectonic setting, metallogenic epochs and deposit types. *Ore Geol. Rev.* **2007**, *31*, 48–87. [[CrossRef](#)]
170. Ou, J.J. Geological Characteristics and Prospecting Direction of Lannitang Porphyry Copper Deposit in Shangri-La, Yunnan. Master's Thesis, Chengdu University of Technology, Chengdu, China, 2014.
171. Li, W.C.; Zeng, P.S.; Hou, Z.Q.; White, N.C. The Pulang porphyry copper deposit and associated felsic intrusions in Yunnan Province, Southwest China. *Econ. Geol.* **2011**, *106*, 79–92.
172. Xu, L.L. The Diagenetic and Metallogenic Geochronology and Magmatic $f\text{O}_2$ Characteristics of Jinshajiang-Red River Porphyry Cu (Mo-Au) Metallogenic Systems. Ph.D. Thesis, Chinese Academy of Sciences, Guiyang, China, 2011.
173. Guan, Y. Relationship between 3D Tectonic Frame and Metallogenic District: Theory and Implications in the Three Rivers Region, Yunnan. Ph.D. Thesis, Chinese Academy of Geological Science, Beijing, China, 2005.
174. Chen, J.L.; Xu, J.F.; Ren, J.B.; Huang, X.X.; Wang, B.D. Geochronology and geochemical characteristics of Late Triassic porphyritic rocks from the Zhongdian arc, eastern Tibet, and their tectonic and metallogenic implication. *Gondwana Res.* **2014**, *26*, 492–504. [[CrossRef](#)]
175. Liu, X.L. The Research on Porphyry Copper Metallogenic System and Post-Ore Modification Preservation since the Indosinian in Geza Arc, Yunnan, SW China. Ph.D. Thesis, China University of Geosciences, Wuhan, China, 2013.
176. Gao, X. The Late Cretaceous Polymetallic Mineralization Related to Granitoid Systems in the Yidun Terrane, East Tibet. Ph.D. Thesis, China University of Geosciences, Beijing, China, 2018.
177. Tang, J.X. Study on Mineralization and Deposit Location Prediction of YULONG Porphyry Copper (Molybdenum) Ore in Tibet. Ph.D. Thesis, Chengdu University of Technology, Chengdu, China, 2003.
178. Zeng, P.S.; Mo, X.X.; Yu, X.H. Nd, Sr and Pb isotopic characteristics of the alkaline-rich porphyries in western Yunnan and its compression strike-slip setting. *Acta Petrol. Mineral.* **2002**, *21*, 231–241.
179. Deng, J.; Yang, L.Q.; Ge, L.S.; Yuan, S.S.; Wang, Q.F.; Zhang, J.; Gong, Q.J.; Wang, C.M. Character and post-ore changes, modifications and preservation of Cenozoic alkali-rich porphyry gold metallogenic system in western Yunnan, China. *Acta Petrol. Sin.* **2010**, *26*, 1633–1645.
180. Dong, F.L. Study on Metallogenic Condition and Potentiality of Copper-Gold-Polymetallic Deposits in Weishan-Yongping Mineralization District, Yunnan. Ph.D. Thesis, China University of Geosciences, Beijing, China, 2003.
181. Shi, L.; Chen, J.C. The relation between stanniferous granite and plate motion in Western Yunan. *Reg. Geol. China* **1984**, *10*, 71–83.
182. Shi, L.; Chen, J.C.; Zhang, W.L.; Fan, Y.C. Tectonic Zoning and Genetic Types of Tin-Bearing Granites in Western Yunnan and Their Relationship with Tin Deposits. In *Geology of Tin Deposits in Asia and the Pacific*; Hutchison, C.S., Ed.; Springer: Berlin/Heidelberg, Germany, 1988; pp. 245–252.
183. Wu, S.L.; Ding, S.Y. Characteristics and distribution of geochemical anomalies in western Yunan tin ore belt. *Geophys. Geochem. Explor.* **1990**, *14*, 47–54.